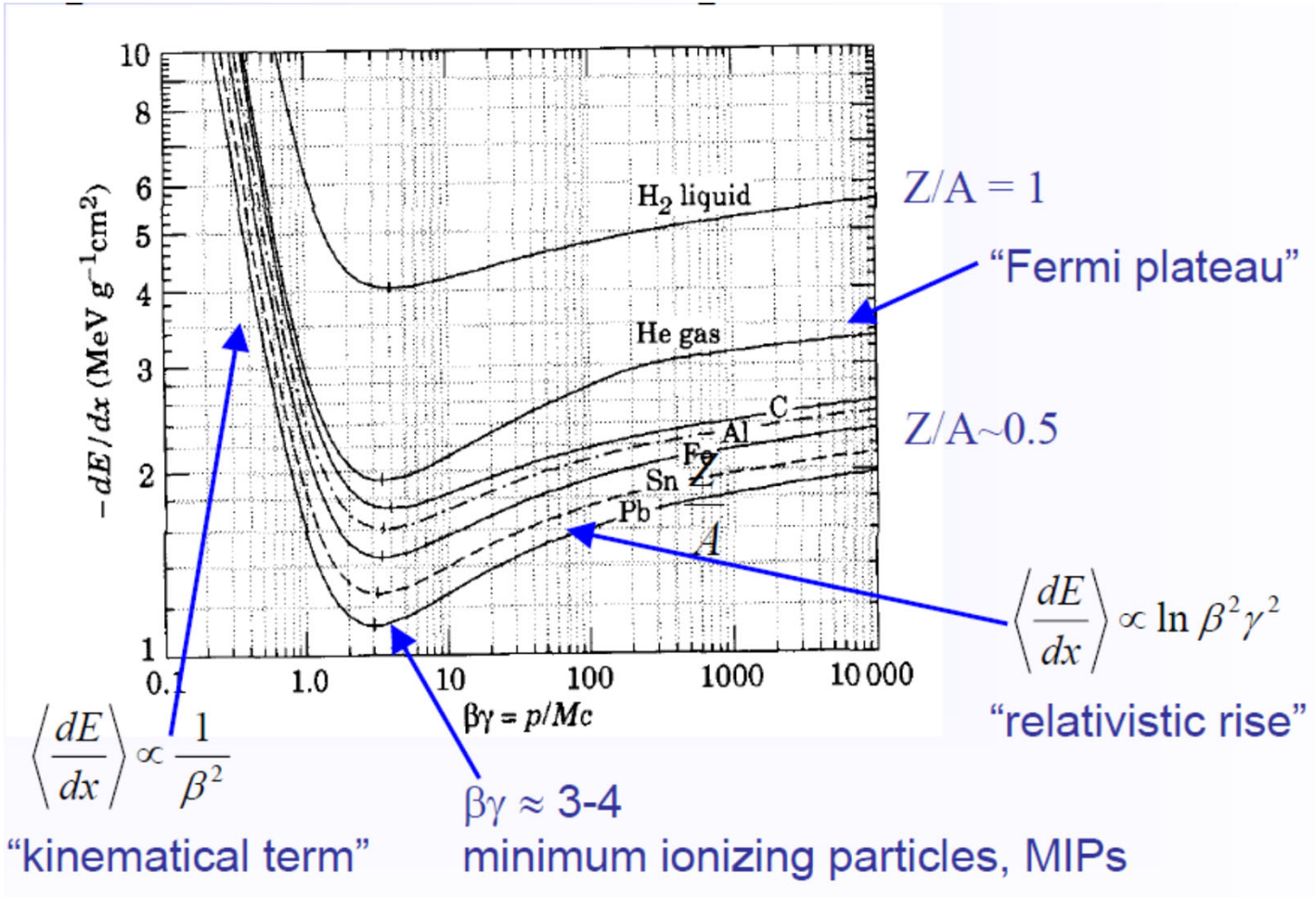

$$-\frac{dE}{dx} = \rho K z^2 \frac{Z}{A}\frac{1}{\beta^2}\left[\ln\frac{2mc^2\beta^2\gamma^2}{I} - \beta^2 - \frac{\delta(\gamma)}{2}\right]$$

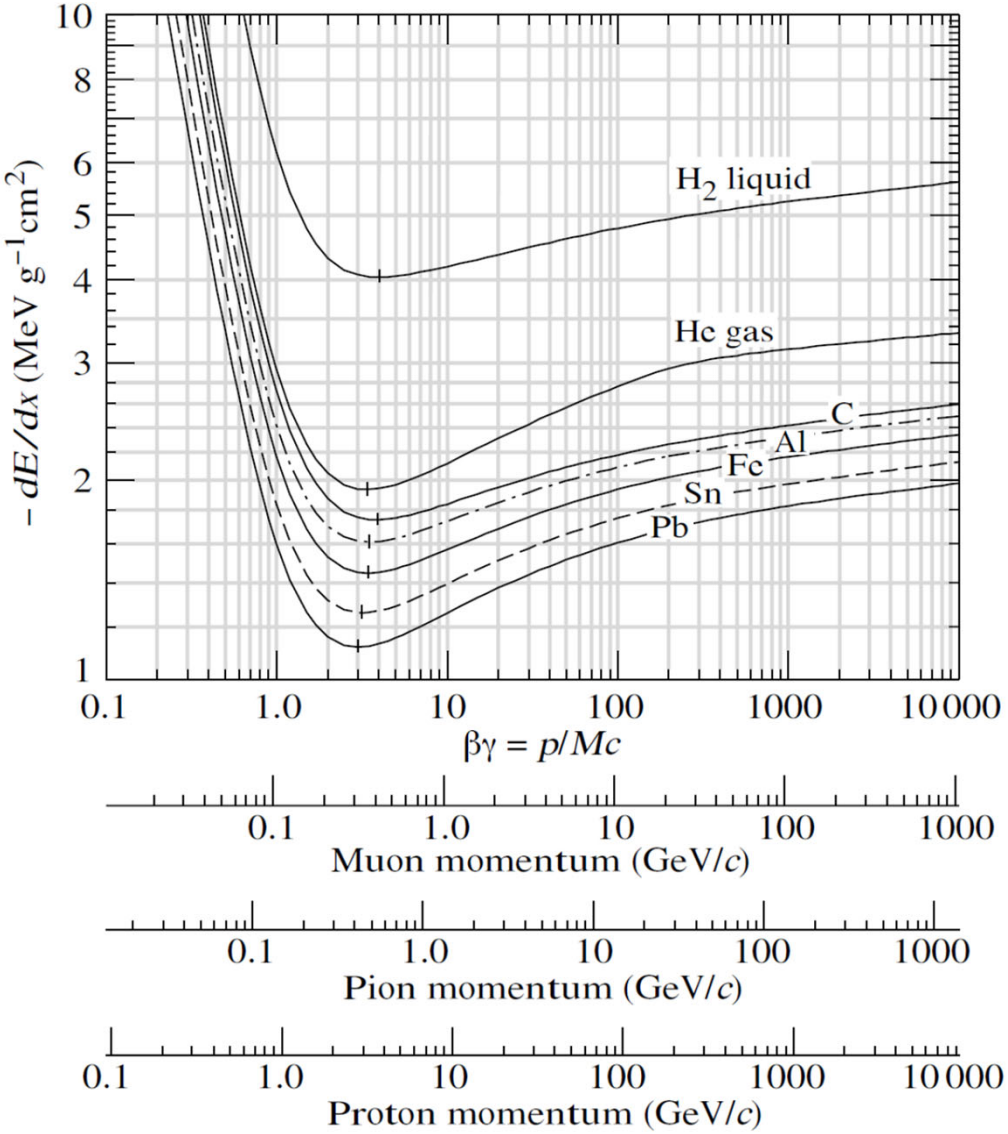
10
8
6
5
4
3
2
1
$-dE/dx$ (MeV g^{-1}cm^2)
H_2 liquid
He gas
C
Al
Fe
Sn
Pb
0.1
1.0
10
100
1000
10 000
$\beta\gamma = p/Mc$
Muon momentum (GeV/c)
Pion momentum (GeV/c)
Proton momentum (GeV/c)

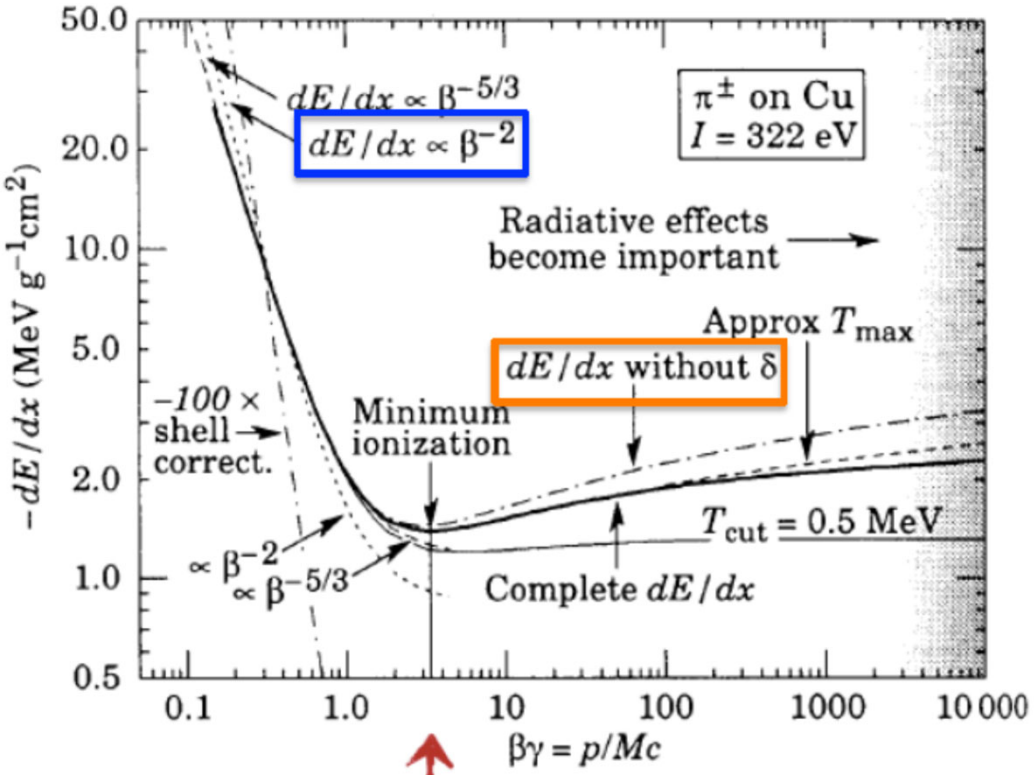

$\beta\gamma = 3\text{-}4$

$$\frac{dE}{dx} \propto \frac{Z^2}{\beta^2} \ln\left(a\beta^2\gamma^2\right)$$

$$\frac{dE}{dx} = Kz^2 \frac{Z}{A}\frac{1}{\beta^2}\left[\frac{1}{2}\ln\frac{2m_e c^2\beta^2\gamma^2 T_{\max}}{I^2} - \beta^2 - \frac{\delta}{2}\right]$$

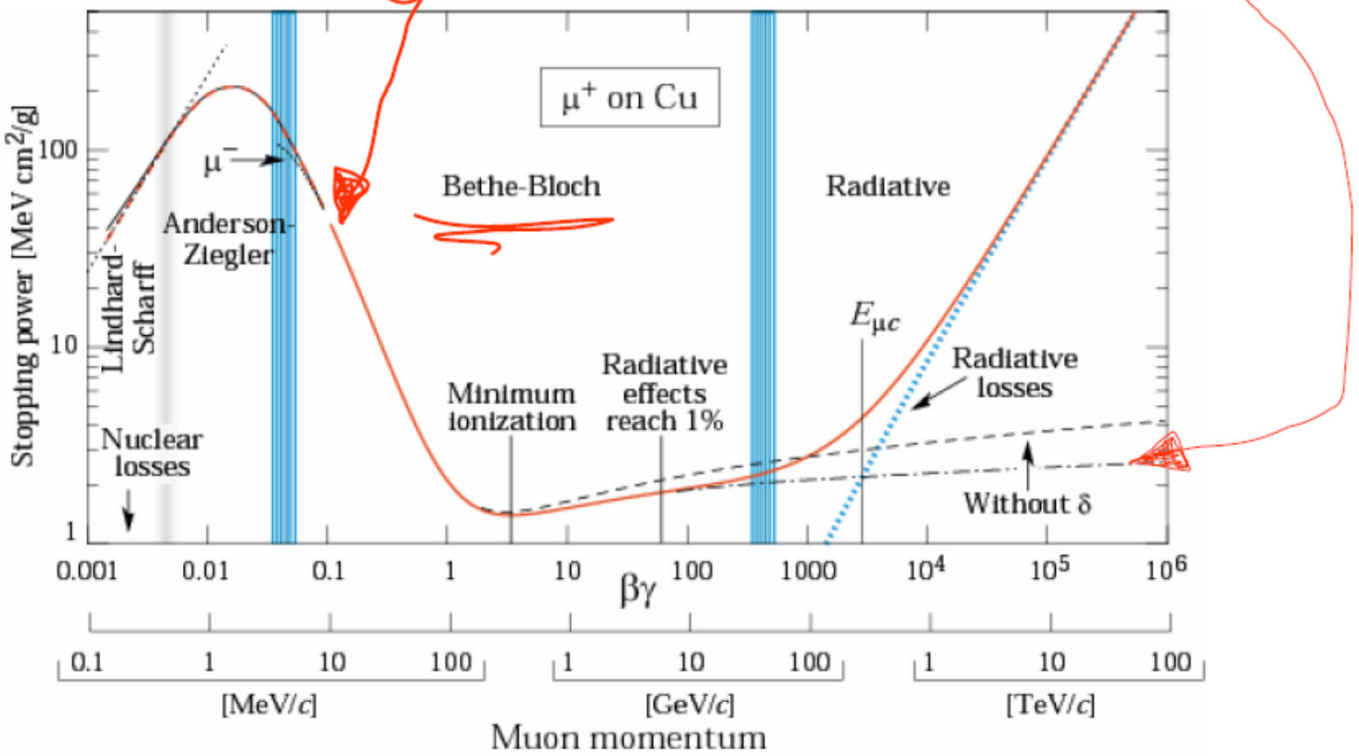

Stopping power (≡⟨dE/dx⟩) for positive muons in copper as a function of $\beta\gamma = p/Mc$ over nine orders of magnitude in momentum (12 orders of magnitude in kinetic energy). Solid curves indicate the total stopping power.

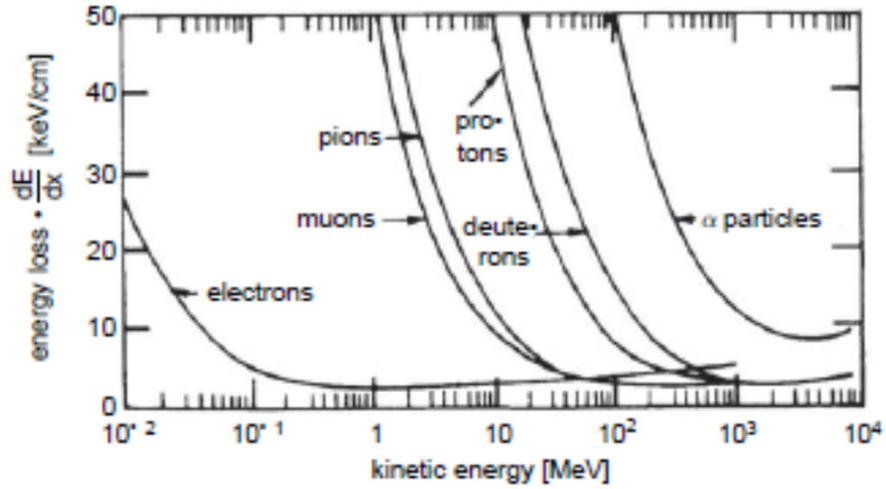

ig. 1.2. Energy loss for electrons, muons, pions, protons, deuterons and α articles in air [14].

- STAR Time-Projection Chamber (TPC):

10% Methan / 90% Argon (2mbar above athm. pressure)

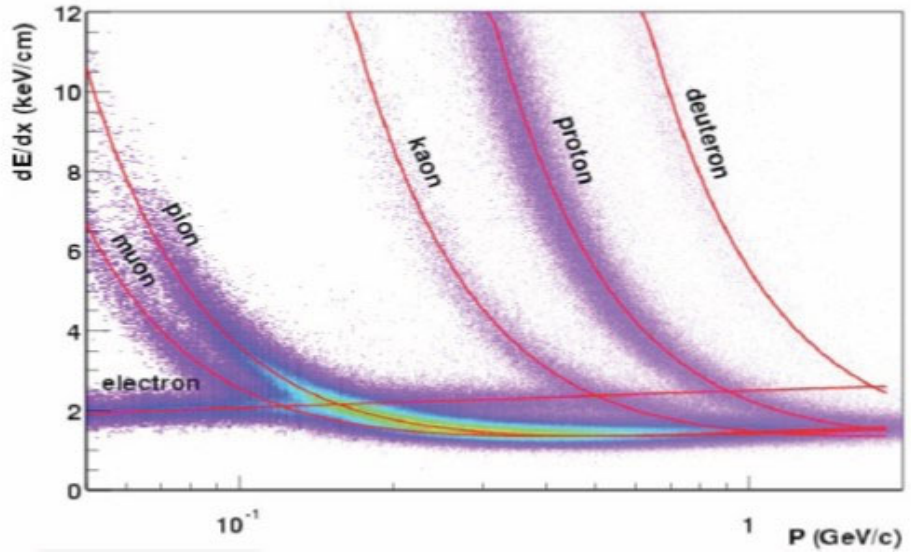

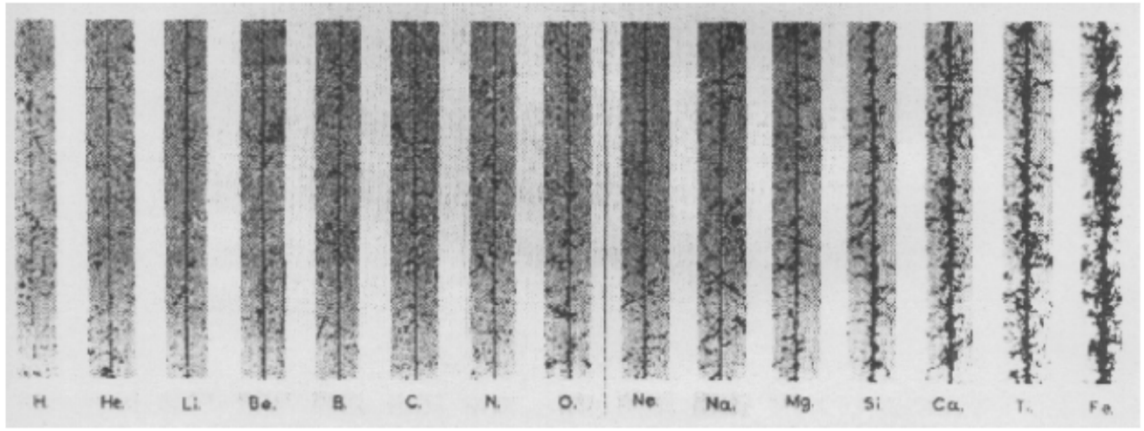
H
He
Li
Be
B
C
N
O
Ne
Na
Mg
Si
Ca
Fe

emulsioni


Scoperta del π
Lattes, Occhialini
e Powell 1947
μ
e
π

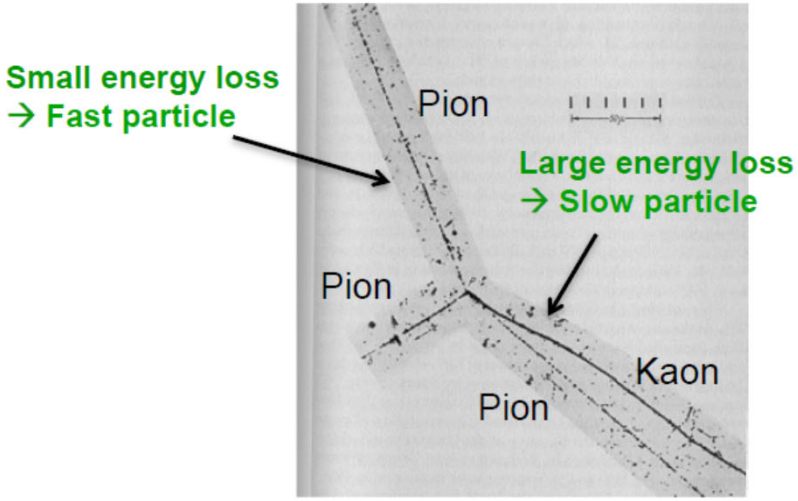
Small energy loss
→ Fast particle
Pion
Large energy loss
→ Slow particle
Pion
Kaon
Pion

Anderson's cloud chamber picture of cosmic radiation from 1932

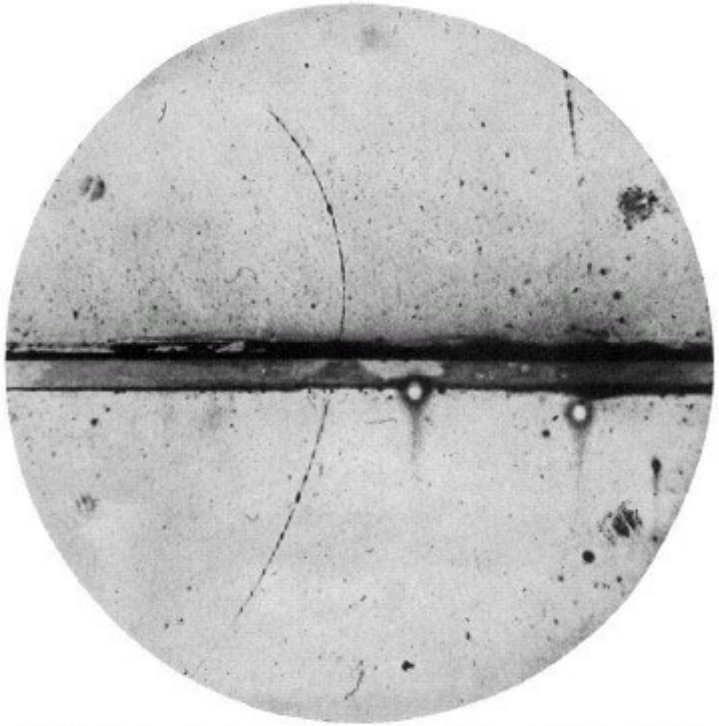

FIG. 1. A 63 million volt positron ($H\rho = 2.1 \times 10^5$ gauss-cm) passing through a 6 mm lead plate and emerging as a 23 million volt positron ($H\rho = 7.5 \times 10^4$ gauss-cm). The length of this latter path is at least ten times greater than the possible length of a proton path of this curvature.

Positron discovery

Charge (and momentum) from the curvature in magn. field (and direction with help of absorber…)
Mass from range vs. momentum

Measured quantities: track, i.e. position measurement (in several points along the trace)

Cloud chamber: sealed environment containing a supersaturated vapor of water or alcohol. When a charged particle interacts with the mixture, it ionizes it. The resulting ions act as condensation nuclei, around which a mist will form .

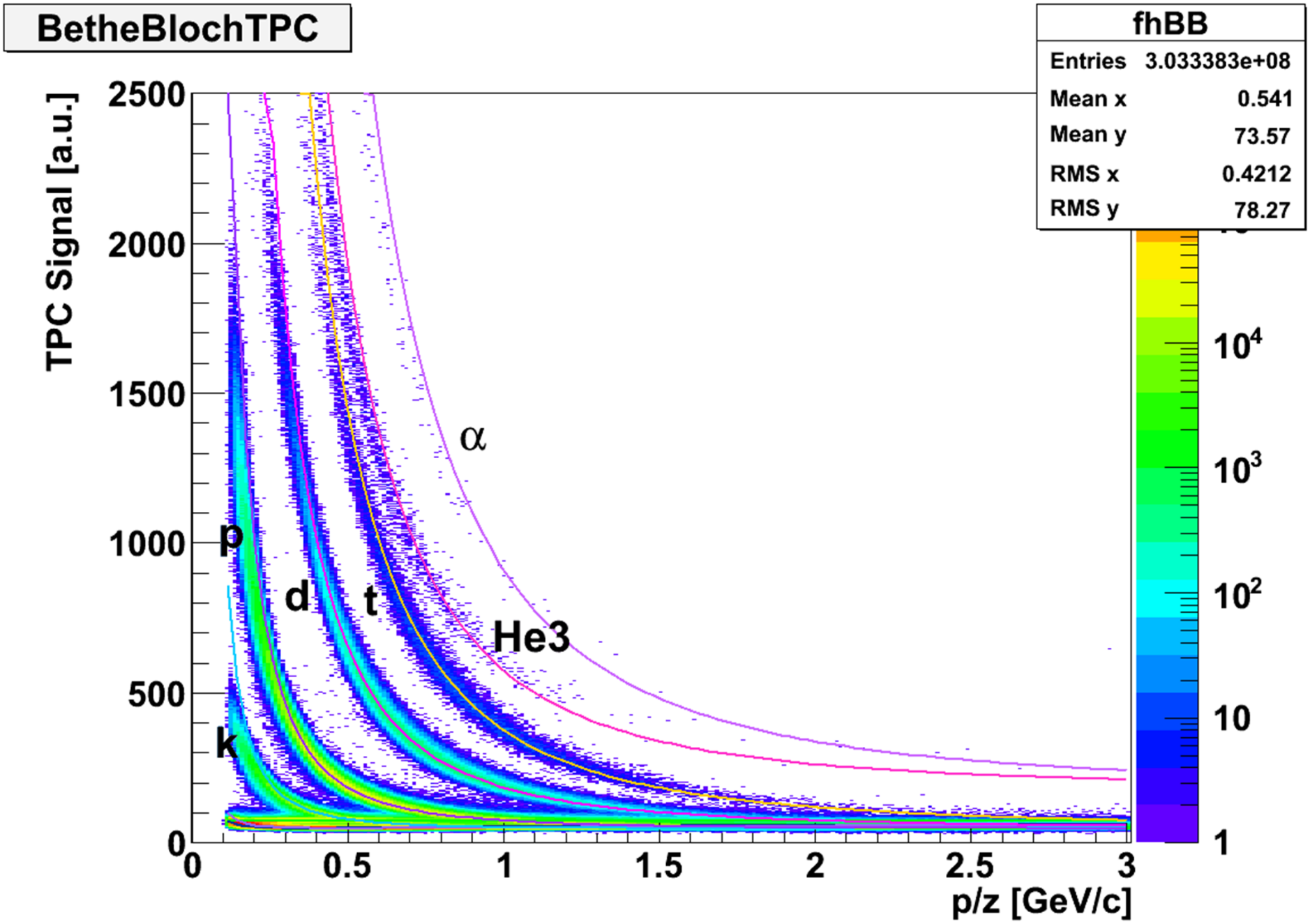
BetheBlochTPC
fhBB
Entries 3.033383e+08
Mean x 0.541
Mean y 73.57
RMS x 0.4212
RMS y 78.27
TPC Signal [a.u.]
p/z [GeV/c]
p
d
t
He3
α
k
0
500
1000
1500
2000
2500
0.5
1
1.5
2
2.5
3
1
10
10^2
10^3
10^4

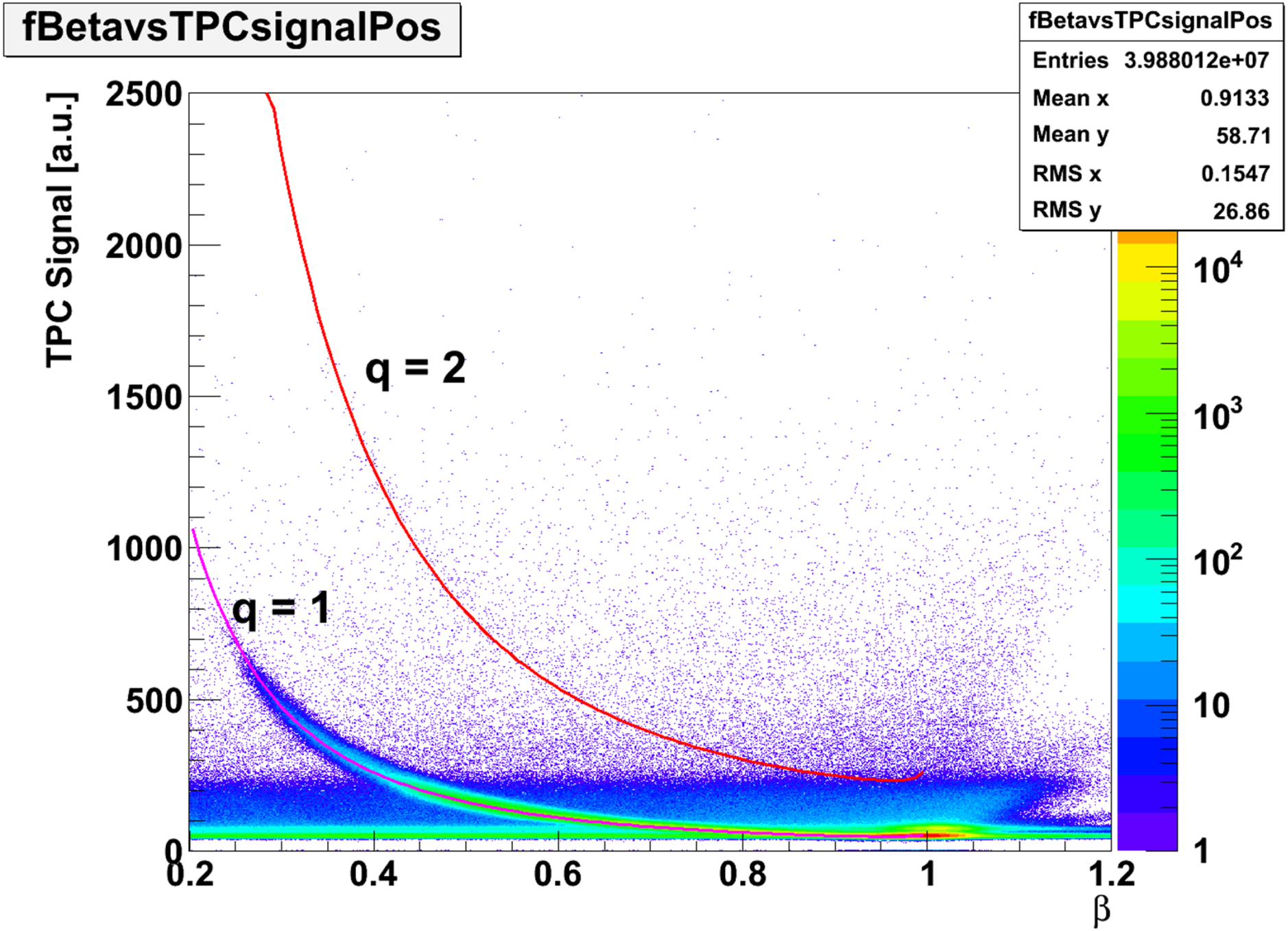
fBetavsTPCsignalPos
fBetavsTPCsignalPos
Entries 3.988012e+07
Mean x 0.9133
Mean y 58.71
RMS x 0.1547
RMS y 26.86
TPC Signal [a.u.]
2500
2000
1500
1000
500
0
q = 2
q = 1
0.2
0.4
0.6
0.8
1
1.2
β
10^4
10^3
10^2
10
1

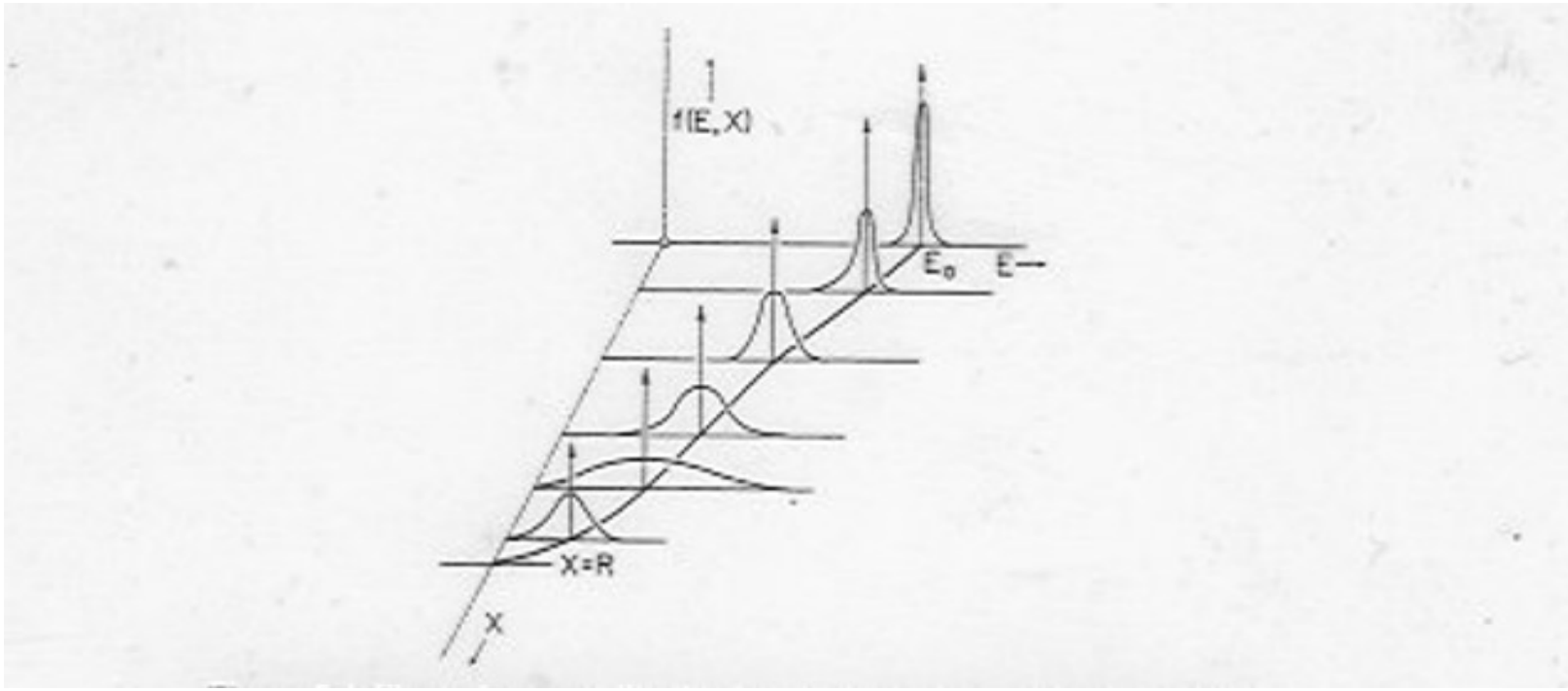
I
I(E,X)
E₀
E
X=R
X

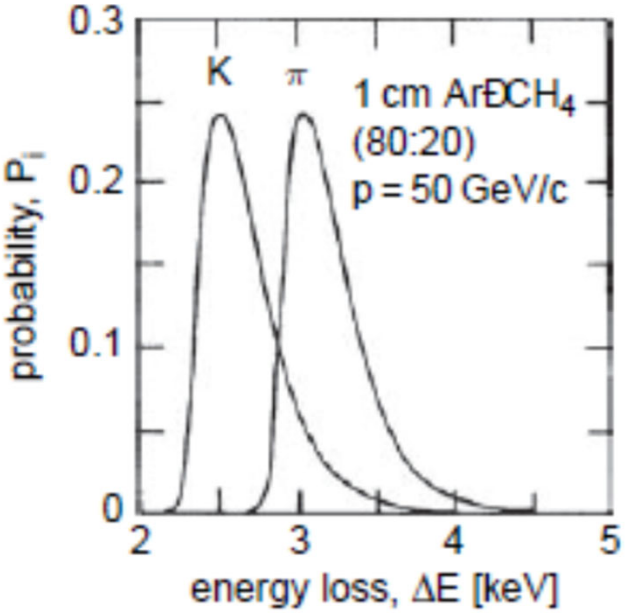

Distribuzione tipica di perdita di energia di pioni e kaoni energia di 50 GeV/c in uno strato di miscela di argon-metano di 1 cm

Protons

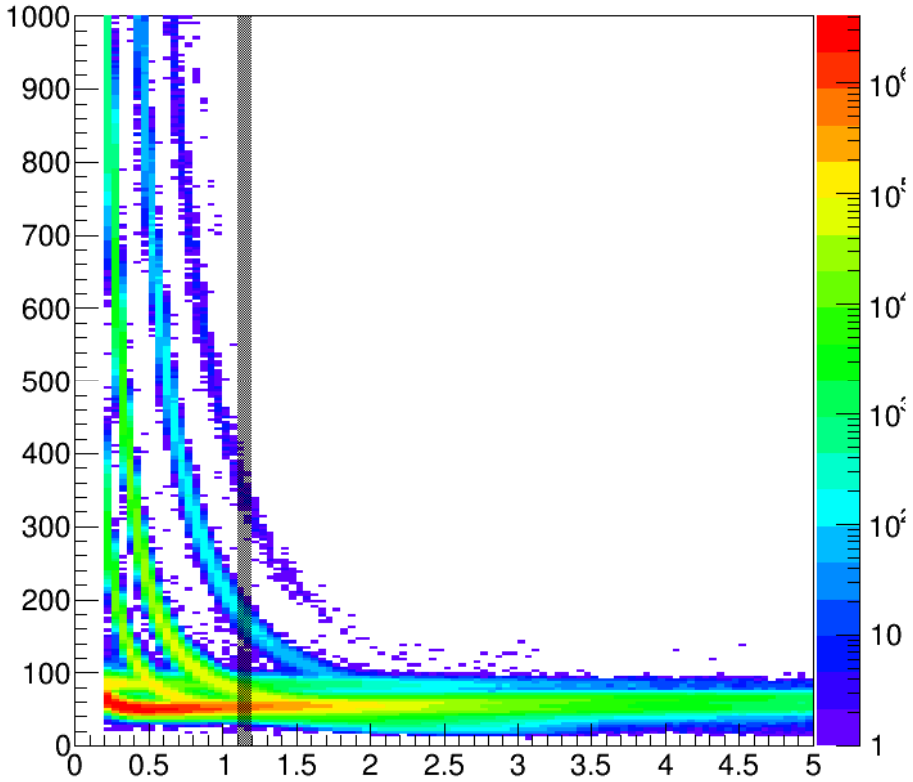

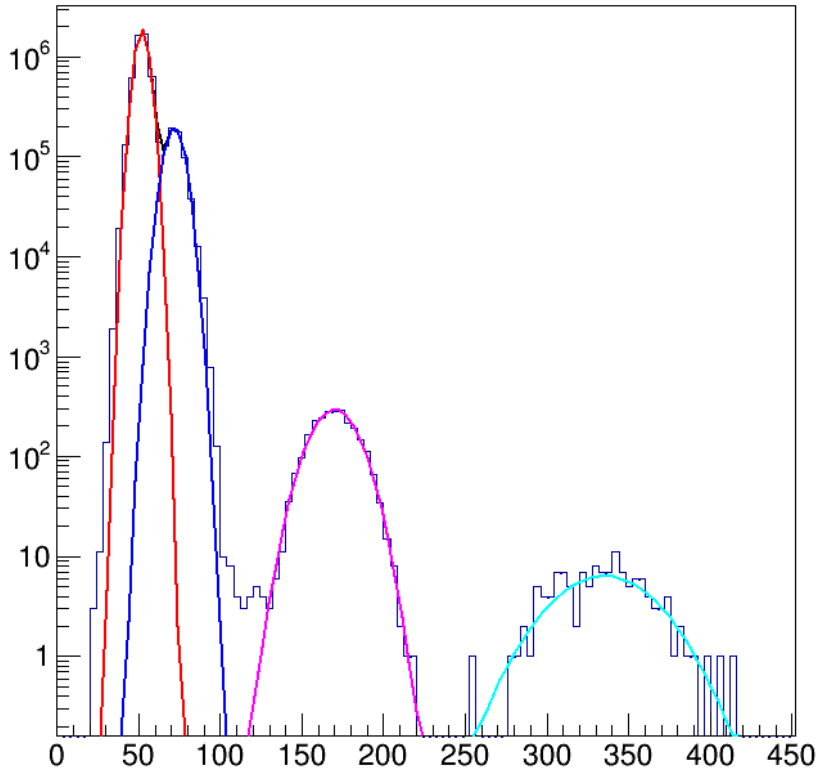

Depth

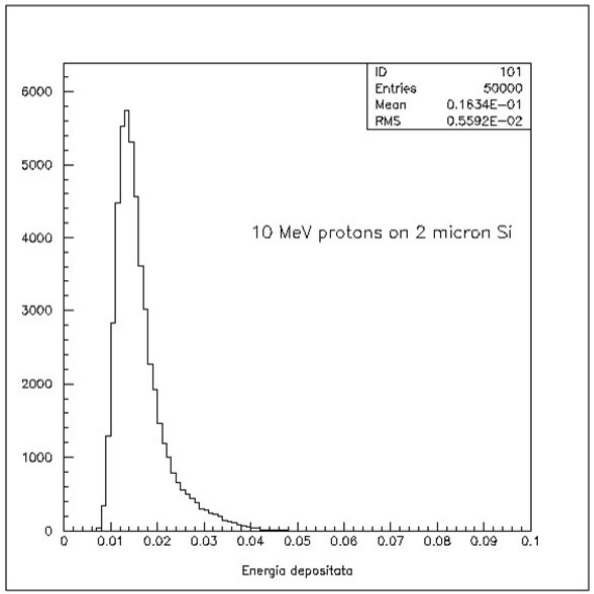
ID 101
Entries 50000
Mean 0.1634E-01
RMS 0.5592E-02
10 MeV protons on 2 micron Si
Energia depositata

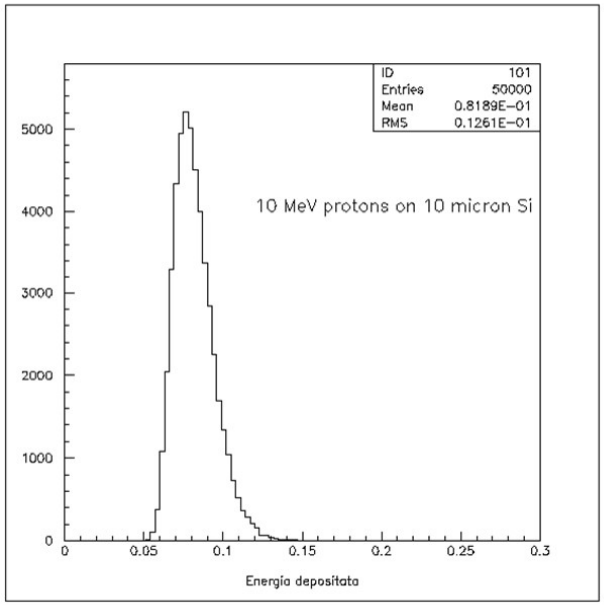
ID 101
Entries 50000
Mean 0.8189E-01
RMS 0.1261E-01
10 MeV protons on 10 micron Si
Energia depositata

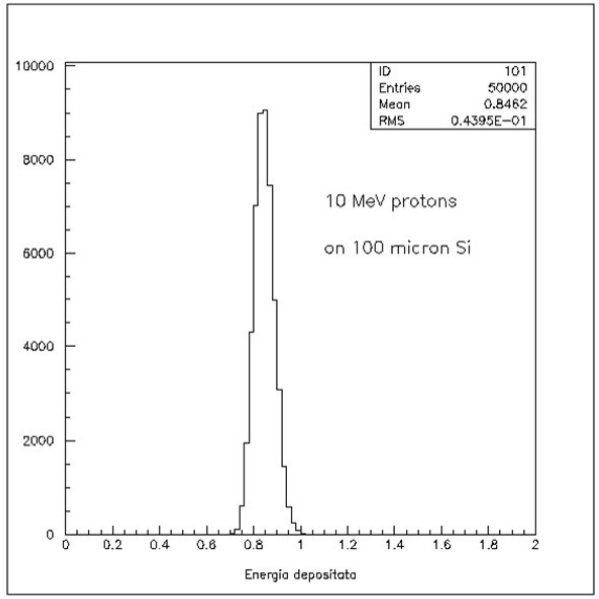
ID 101
Entries 50000
Mean 0.8462
RMS 0.4395E-01
10 MeV protons
on 100 micron Si
Energia depositata

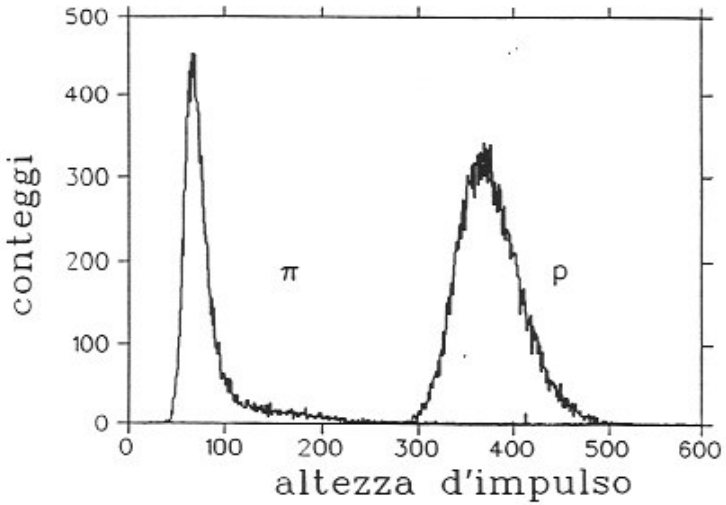

Fig.5.6- Altezza d'impulso di π^+, p in ΔE1 per p=400 MeV/c.

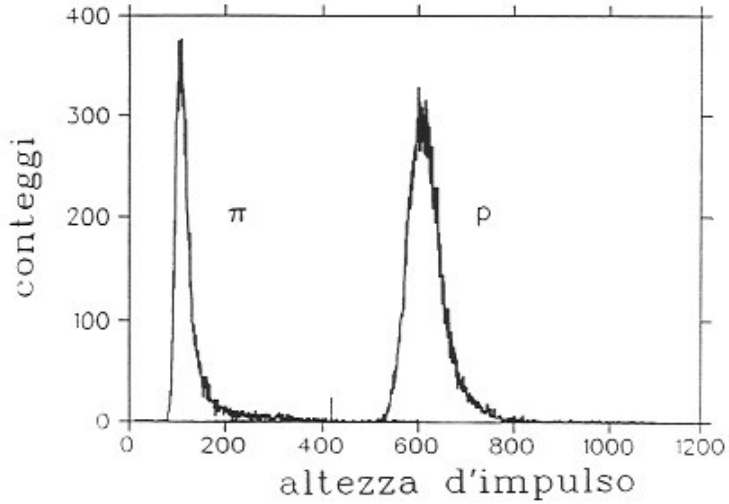

Fig.5.7- Altezza d'impulso di π^+, p in ΔE2 per p=400 MeV/c.

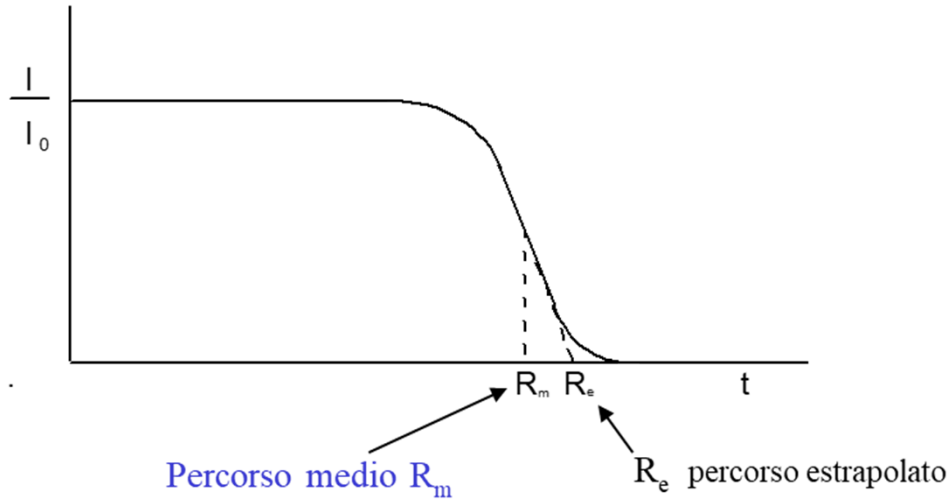
I
I 0
R m
R e
t
Percorso medio R m
R e percorso estrapolato

Mass discrimination also possible by making RANGE measurements

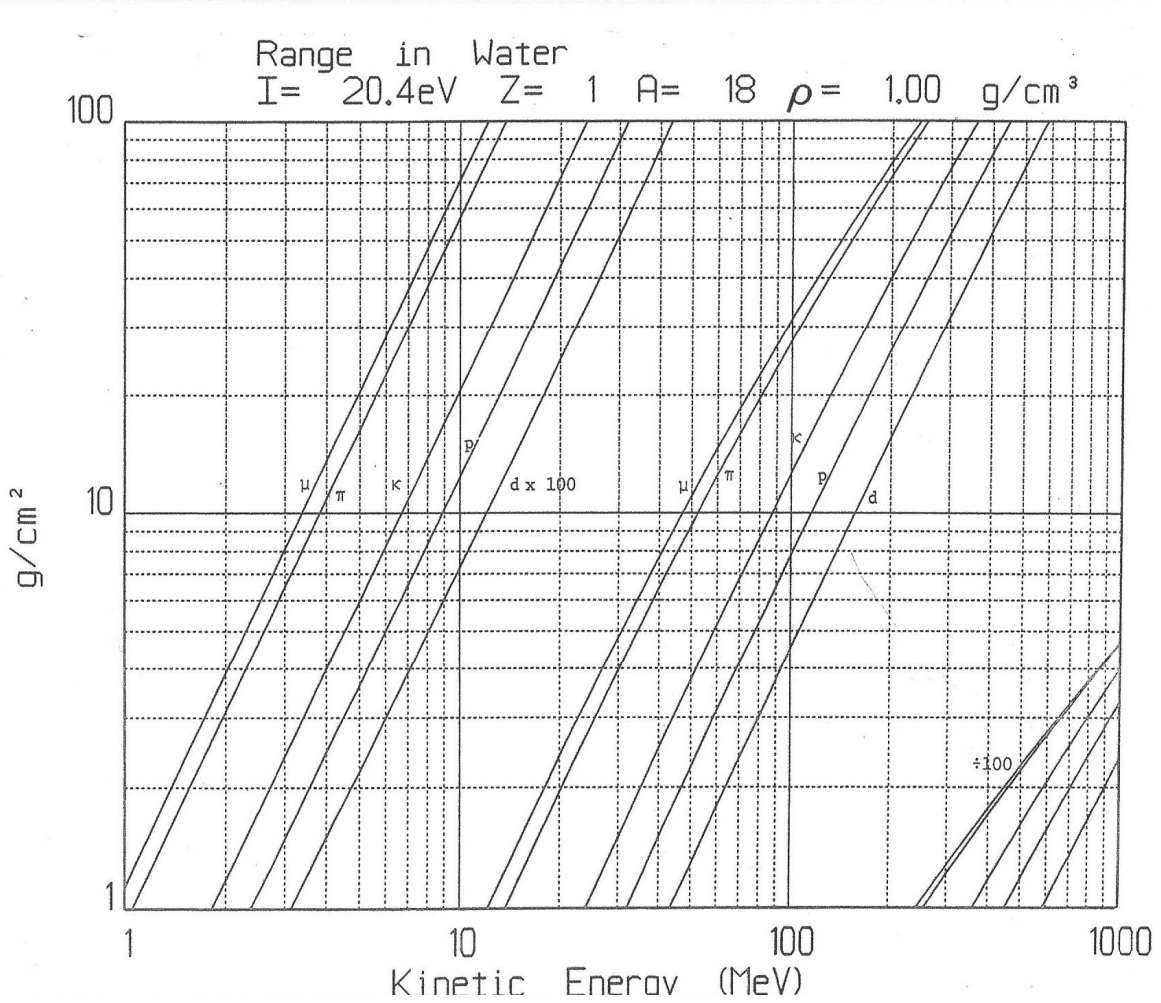

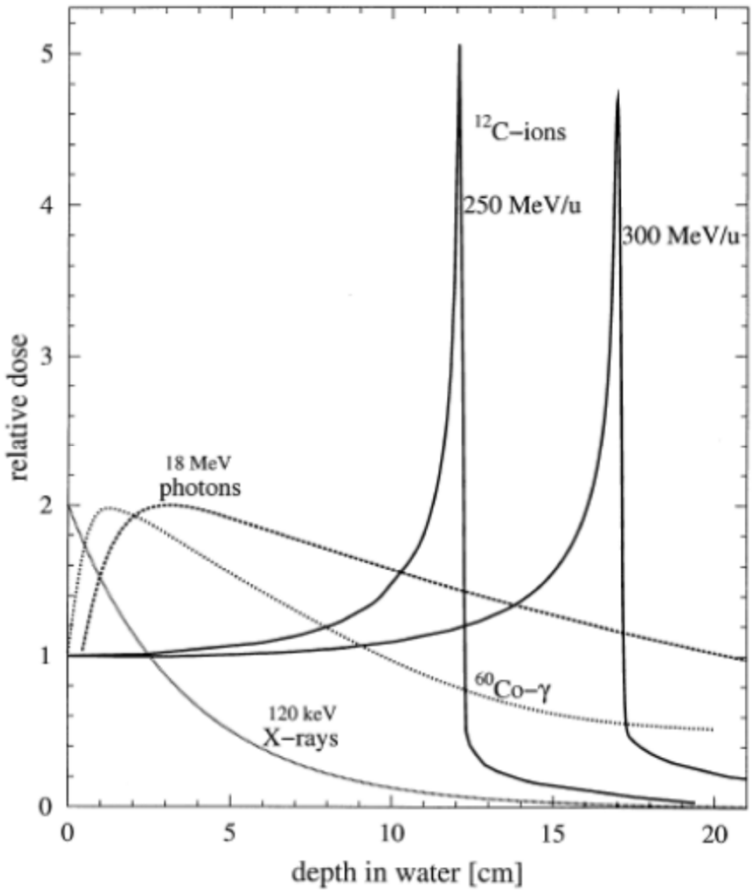
relative dose
depth in water [cm]
0
1
2
3
4
5
0
5
10
15
20
^{12}C–ions
250 MeV/u
300 MeV/u
18 MeV
photons
^{60}Co–γ
120 keV
X–rays

ontherapy.pdf (SECURED) - Adobe Reader

it View Document Tools Window Help

25 / 38 106% Find

Share documents and collaborate live within PDF files

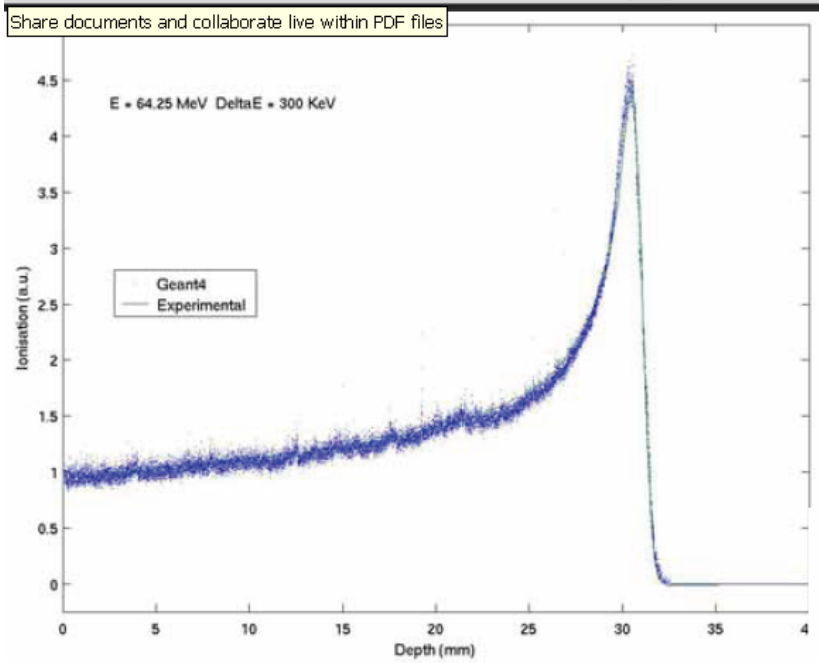

Physic models: comparison vs experimental data

Low energy libraries and hadronic physics

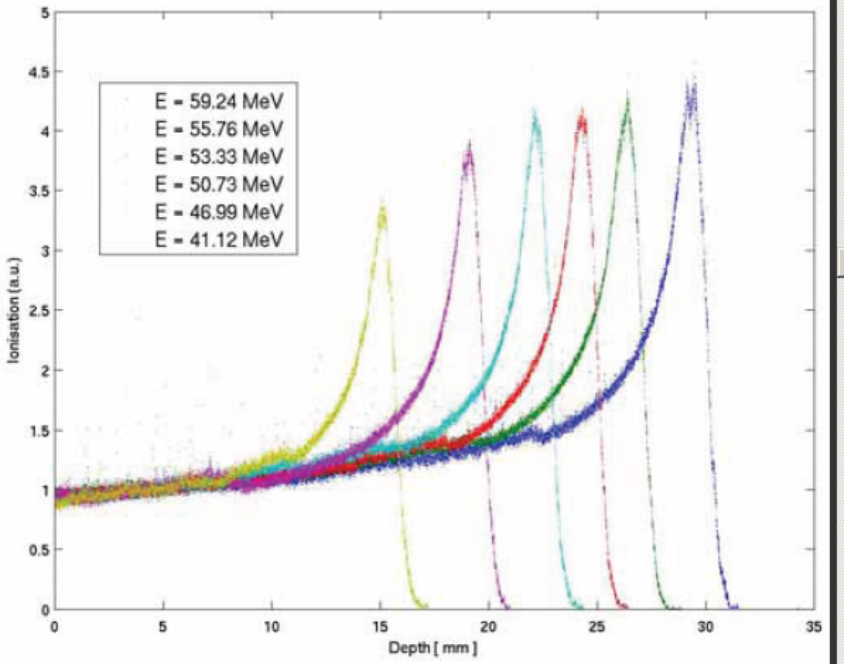

Bragg peaks at diferent energies

G.A.P. Cirrone Phl

RADIAZIONE DI FRENAMENTO

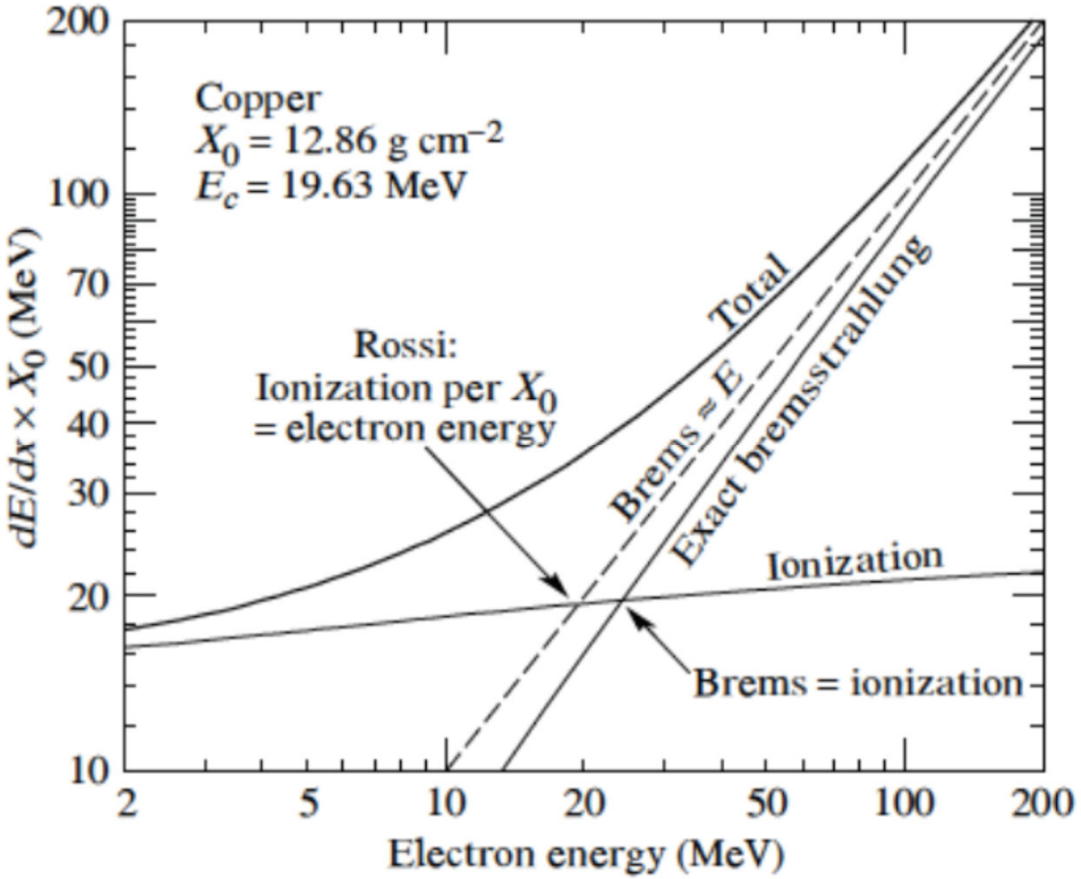

$$\frac{dE}{dx} = Kz^2 \frac{Z}{A}\frac{1}{\beta^2}\left[\frac{1}{2}\ln\frac{2m_e c^2\beta^2\gamma^2 T_{\max}}{I^2} - \beta^2 - \frac{\delta}{2}\right]$$

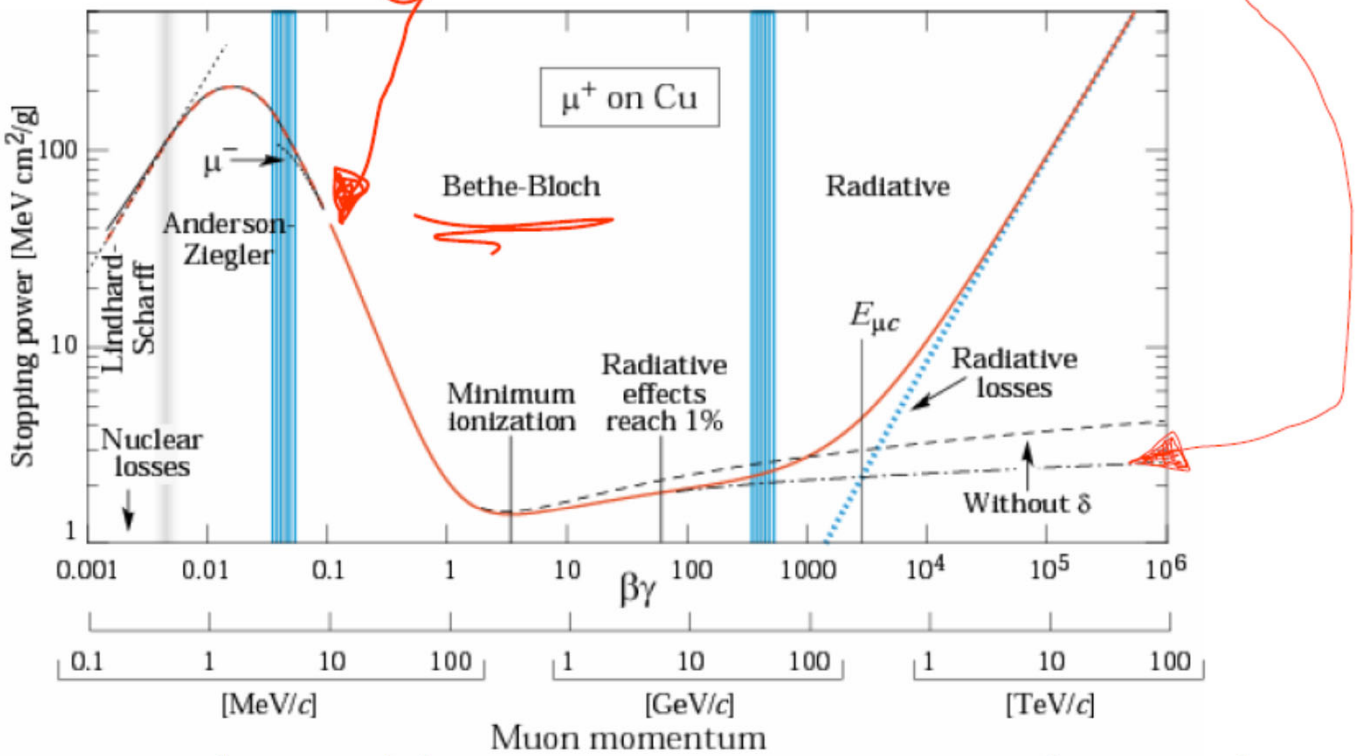

Stopping power (≡⟨dE/dx⟩) for positive muons in copper as a function of βγ =p/Mc over nine orders of magnitude in momentum (12 orders of magnitude in kinetic energy). Solid curves indicate the total stopping power.

the number of photons becomes, after angular integration,

$$\frac{dN}{d\lambda}=\frac{2\pi\alpha}{\lambda^2}L\sin^2\theta_c \tag{5.7}$$

The number of photons emitted in the wavelength interval from λ_1 to λ_2 is then

$$N=2\pi\alpha L\int_{\lambda_2}^{\lambda_1}\sin^2\theta_c/\lambda^2\,d\lambda \tag{5.8}$$

For a counter equipped with a photocathode sensitive in the visible region, $\lambda_1=400$ nm and $\lambda_2=700$ nm, such that we have

$$\frac{N}{L}=490\sin^2\theta_c \quad \text{photons/cm}$$

If the sensitivity is expanded into the ultraviolet region, the yield of photons can be increased by a factor of two to three. One way of achieving this goal

Fig. 5.6. Cherenkov angle θ_c as a function of the reduced particle velocity $\beta=v/c$ for a series of refractive indices n.

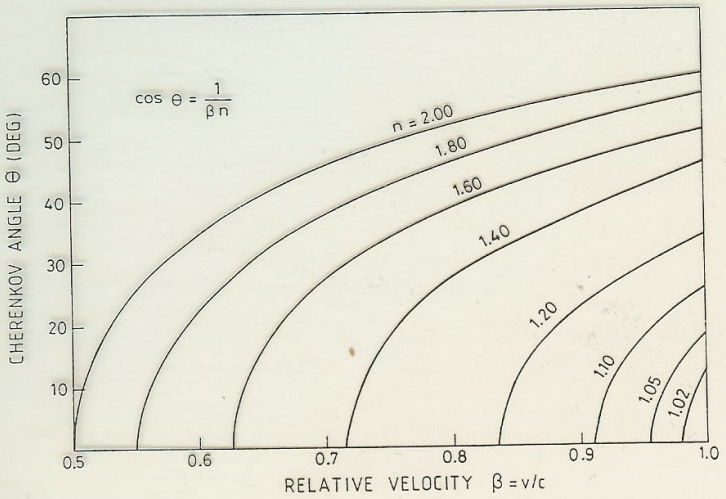

Table 6.2. *Compilation of Cherenkov radiators [1, 34, 35, 122]. The index of refraction for gases is for 0 °C and 1 atm (STP). Solid sodium is transparent for wavelengths below 2000 Å [447, 448]*

material	$n-1$	β-threshold	γ-threshold
solid sodium	3.22	0.24	1.029
lead sulfite	2.91	0.26	1.034
diamond	1.42	0.41	1.10
zinc sulfide (ZnS(Ag))	1.37	0.42	1.10
silver chloride	1.07	0.48	1.14
flint glass (SFS1)	0.92	0.52	1.17
lead fluoride	0.80	0.55	1.20
Clerici solution	0.69	0.59	1.24
lead glass	0.67	0.60	1.25
thallium formate solution	0.59	0.63	1.29
scintillator	0.58	0.63	1.29
Plexiglas (lucite)	0.48	0.66	1.33
boron silicate glass (Pyrex)	0.47	0.68	1.36
water	0.33	0.75	1.52
silica aerogel	0.025 - 0.075	0.93 - 0.976	4.5 - 2.7
pentane (STP)	$1.7 \cdot 10^{-3}$	0.9983	17.2
CO_2 (STP)	$4.3 \cdot 10^{-4}$	0.9996	34.1
air (STP)	$2.93 \cdot 10^{-4}$	0.9997	41.2
H_2 (STP)	$1.4 \cdot 10^{-4}$	0.99986	59.8
He (STP)	$3.3 \cdot 10^{-5}$	0.99997	123

supposed to be precisely at threshold and does not radiate. Under these circumstances one has:

$$\beta_2 = \frac{1}{n} \tag{6.26}$$

or

$$\gamma_2 = \frac{1}{\sqrt{1-\frac{1}{n^2}}} \,. \tag{6.27}$$

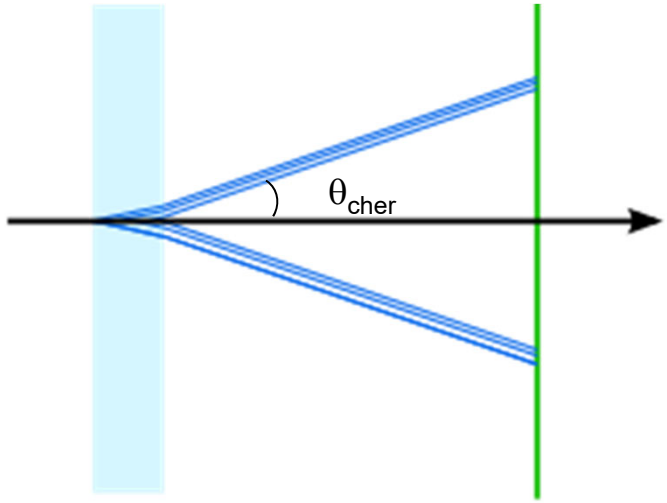
θ_{cher}
RADIATORE
SCHERMO FOTOSENSIBILE

Development of a RICH detector for electron identification in CBM (FAIR/GSI)

UrQMD simulation of central Au+Au collisions, 25 AGeV

event display of inner fraction of RICH detector:

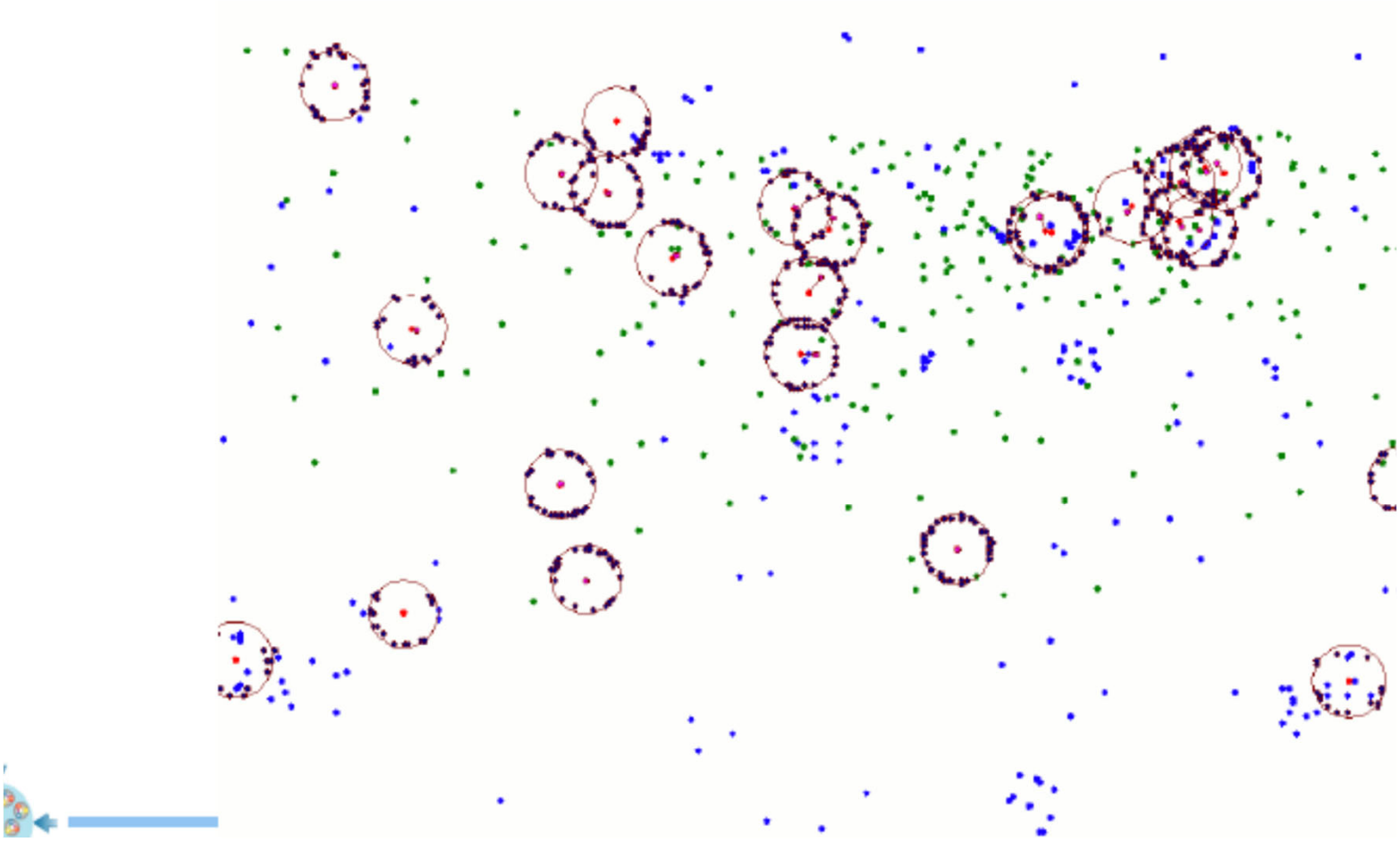

Ice cube
Pictorial event

Selecting events coming from ‘below’
(using the earth as a filter/shield)

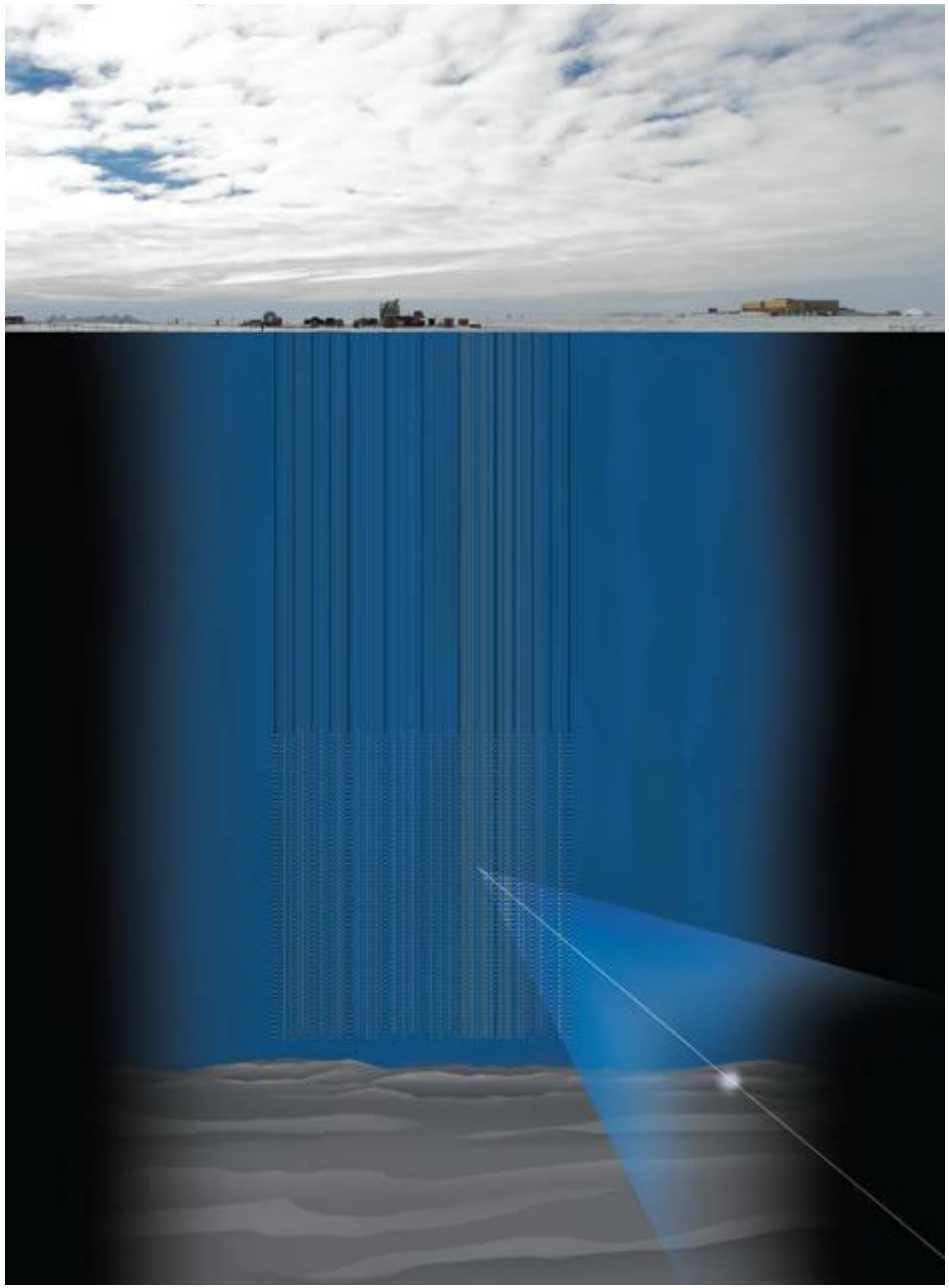

Inserire figura con % relativa ass foto, compt etc per diversi Z..

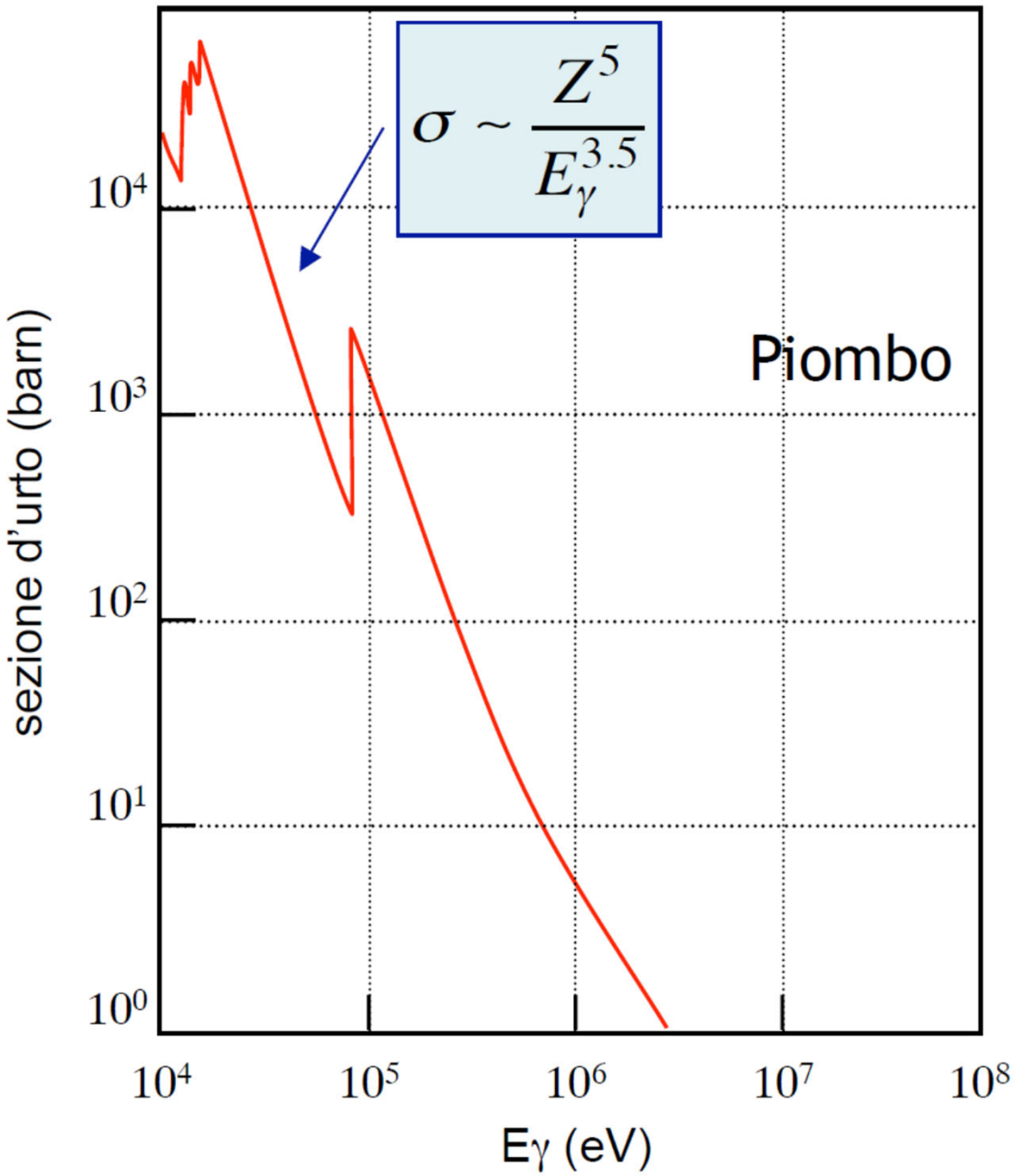
$\sigma \sim \frac{Z^5}{E_\gamma^{3.5}}$
Piombo
sezione d'urto (barn)
10^4
10^3
10^2
10^1
10^0
10^4
10^5
10^6
10^7
10^8
Eγ (eV)

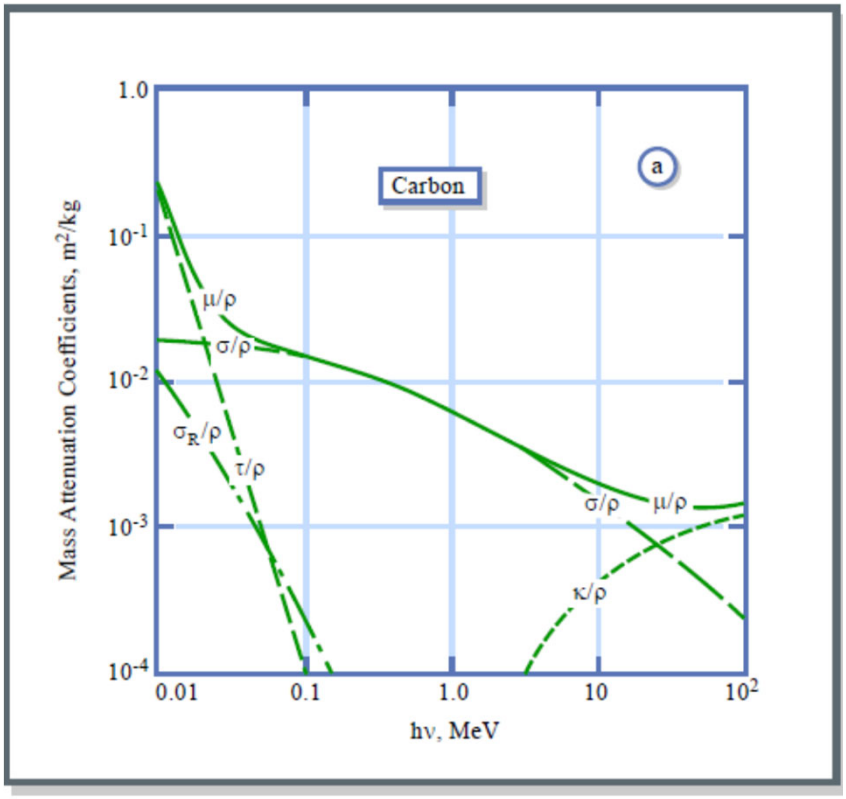

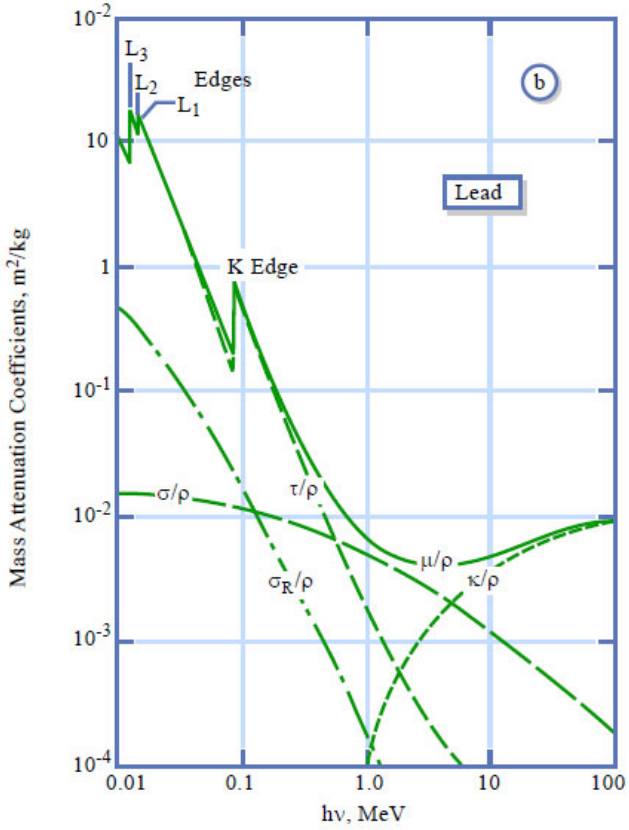

Mass attenuation coefficients for carbon (a) and lead (b). τ/ρ indicates the contribution of the photoelectric effect, σ/ρ is that of the Compton effect, κ/ρ that of pair production, and σ_R/ρ that of Rayleigh (coherent) scattering. μ/ρ is their sum, which is closely approximated in Pb by the τ/ρ curve below $h\nu = 0.1$ MeV.

Interaction of Photons with Matter

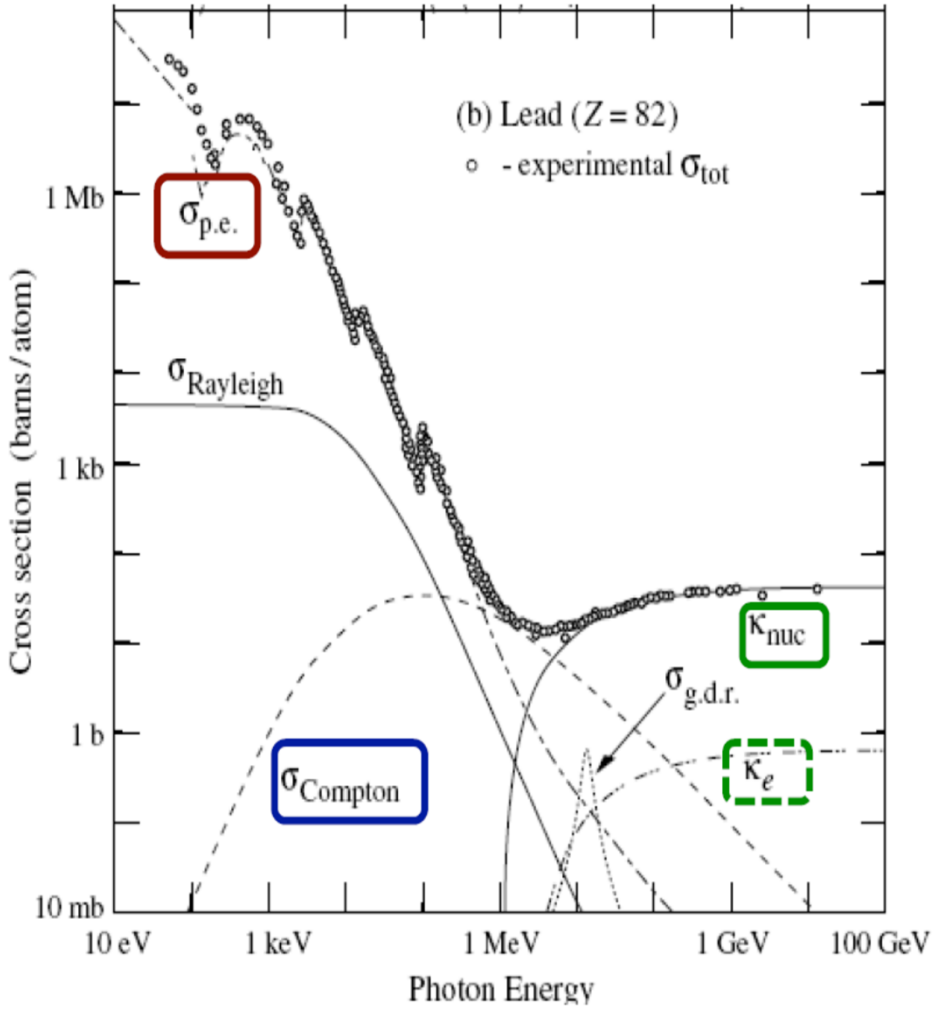

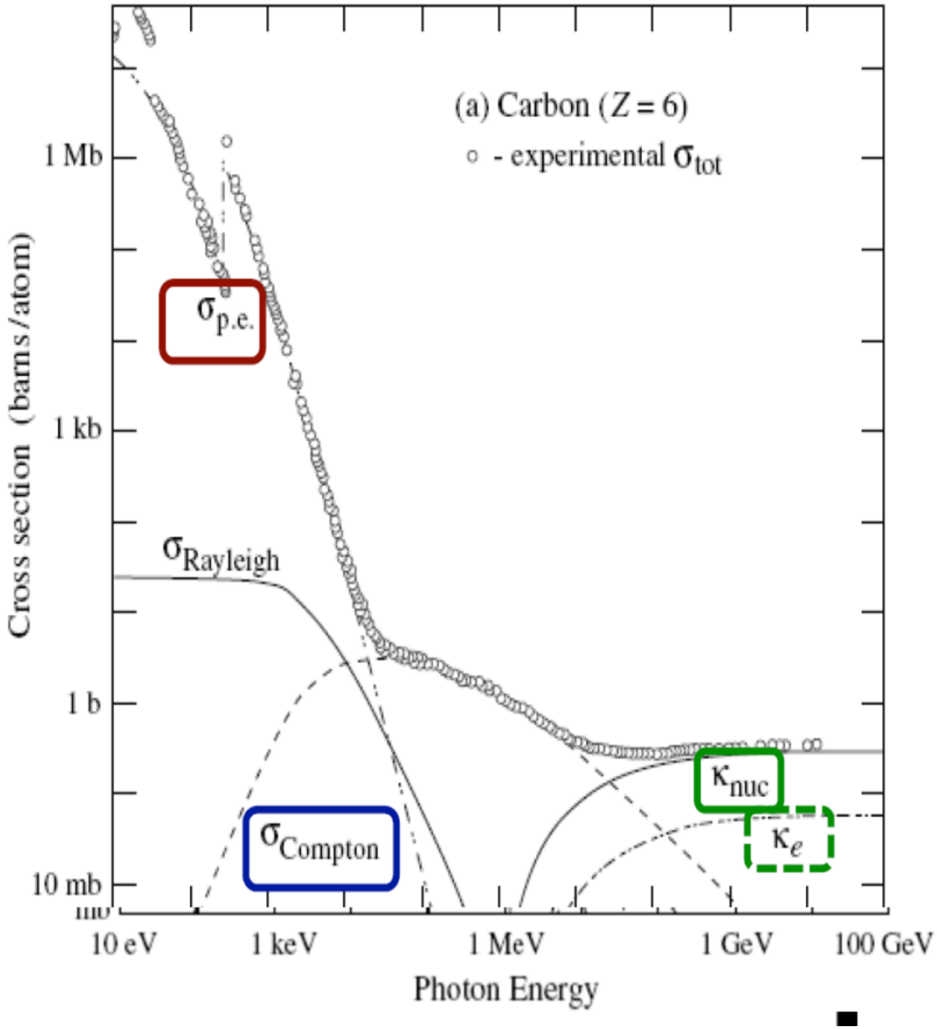

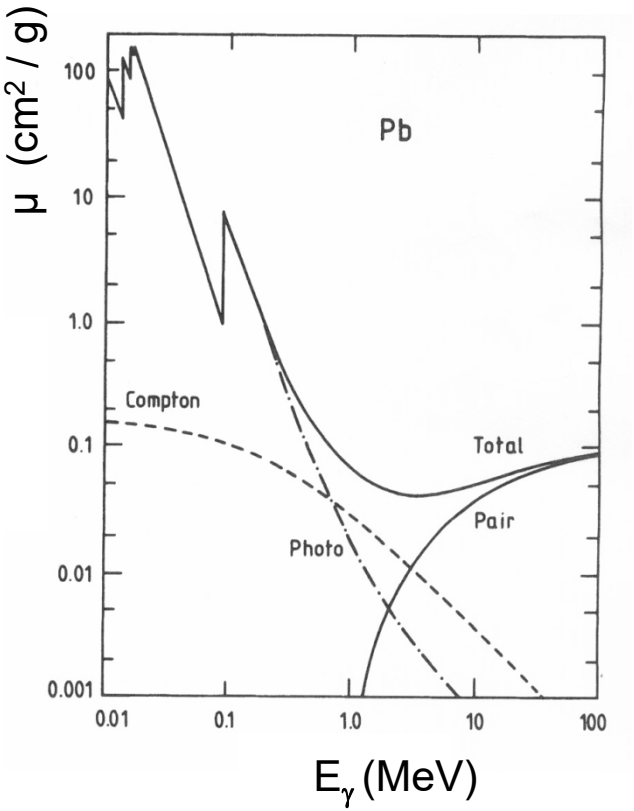
μ (cm² / g)
Pb
Compton
Photo
Pair
Total
100
10
1.0
0.1
0.01
0.001
0.01
0.1
1.0
10
100
Eγ (MeV)

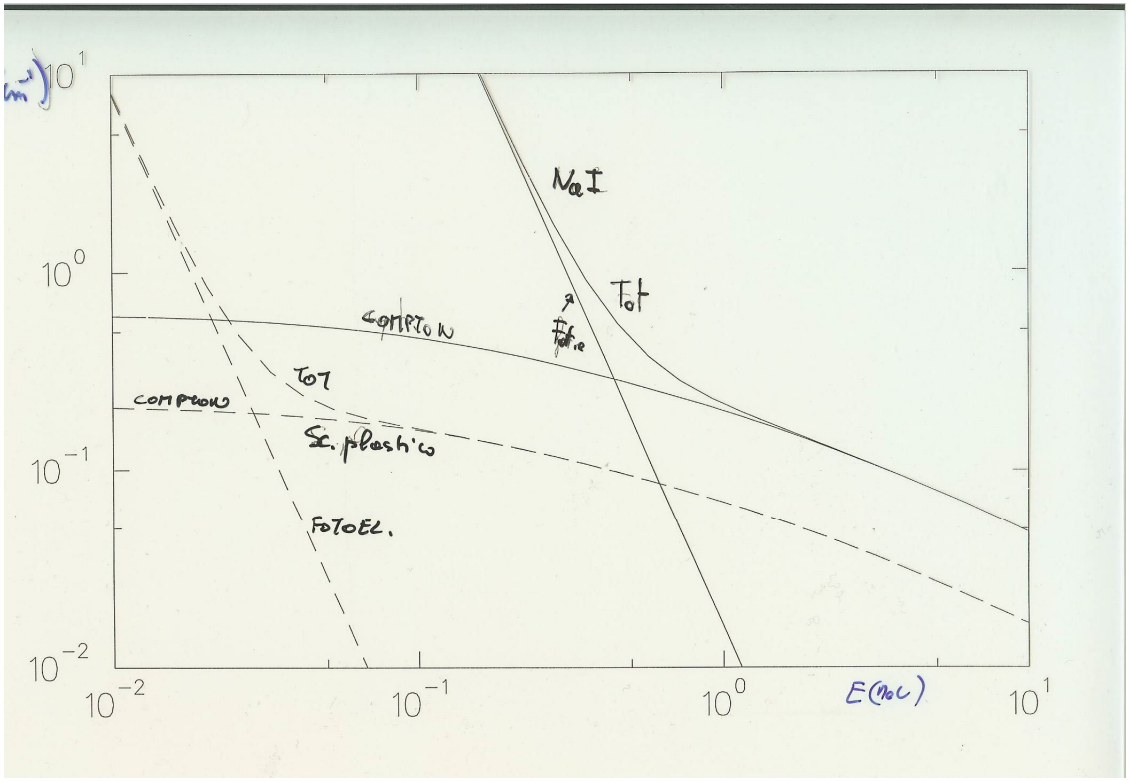
NaI
Tot
COMPTON
Tot
COMPTON
Sc. plastico
FOTOEL.
E(MeV)

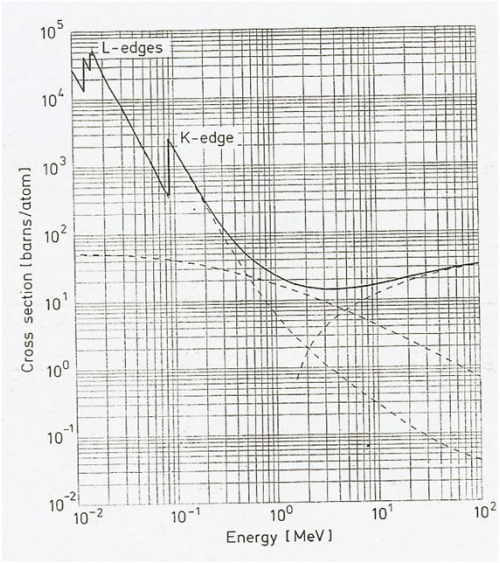
L-edges
K-edge
Cross section [barns/atom]
Energy [MeV]

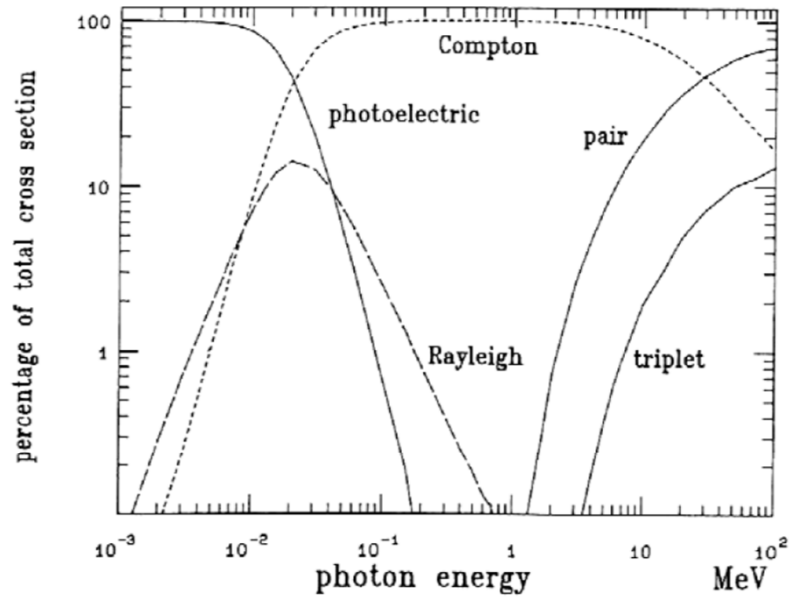

Fig. 11. Percentage contribution of various photon interactions to the total cross section of carbon as a function of photon energy. Data are from the EGS4 system (Nelson *et al.*, 1985) and Hubbell (1969) for the triplet component.

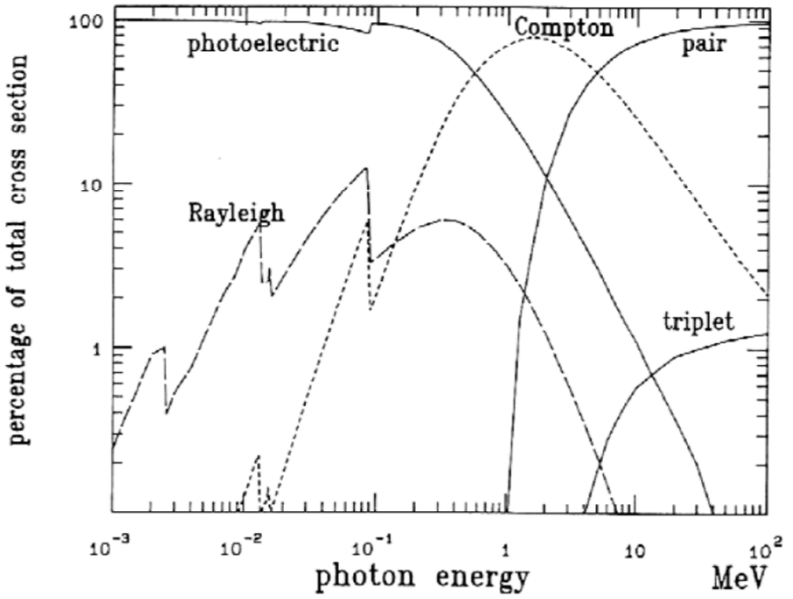

Fig. 12. Percentage contribution of various photon interactions to the total cross section of lead as a function of photon energy. Data are from the EGS4 system (Nelson *et al.*, 1985)

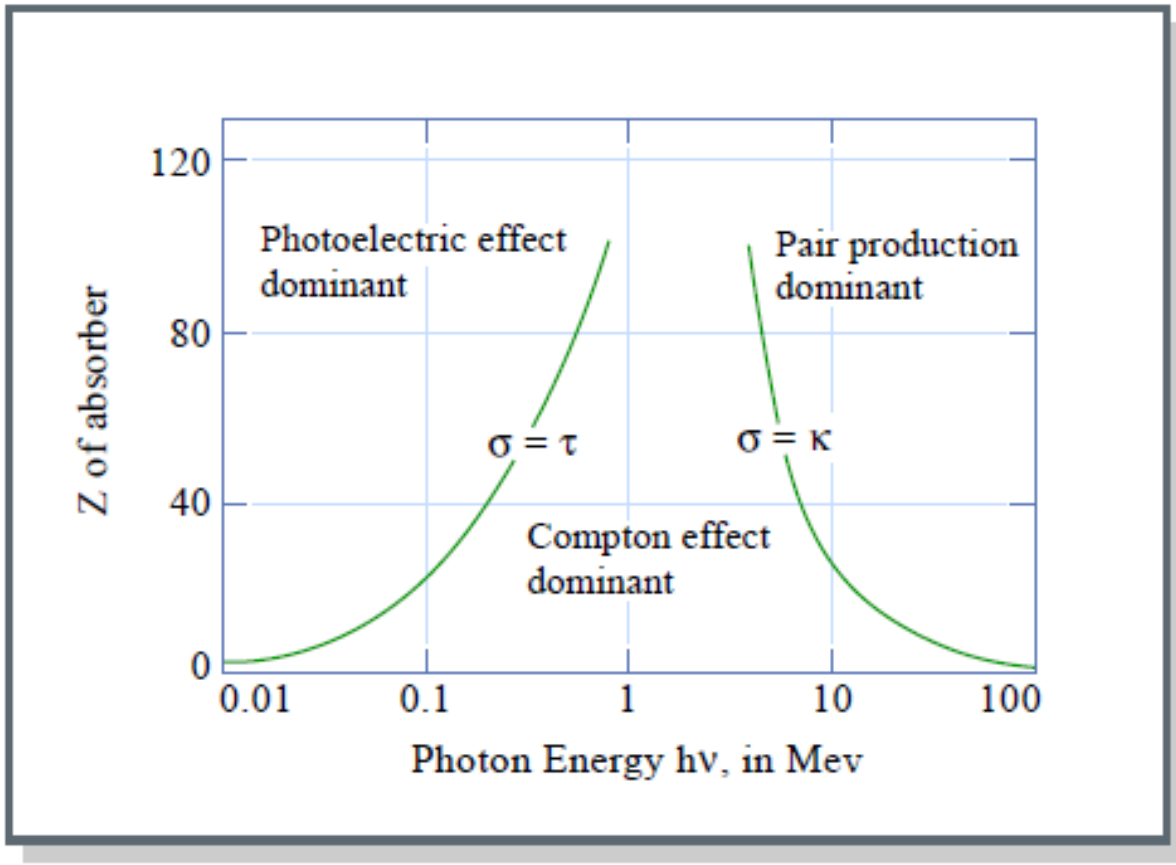

Figure by MIT OCW.

Photon Absorption Length λ

Definition of mass absorption coefficient: $\lambda = \frac{1}{(\mu/\rho)}$ [g cm^{-2}]

$\sigma_{Ph} \propto \frac{Z^5}{E^{3.5}}$ $\sigma_{Compton} \propto \frac{\ln E}{E} \cdot Z$ $\sigma_{Pair} \propto Z^2$

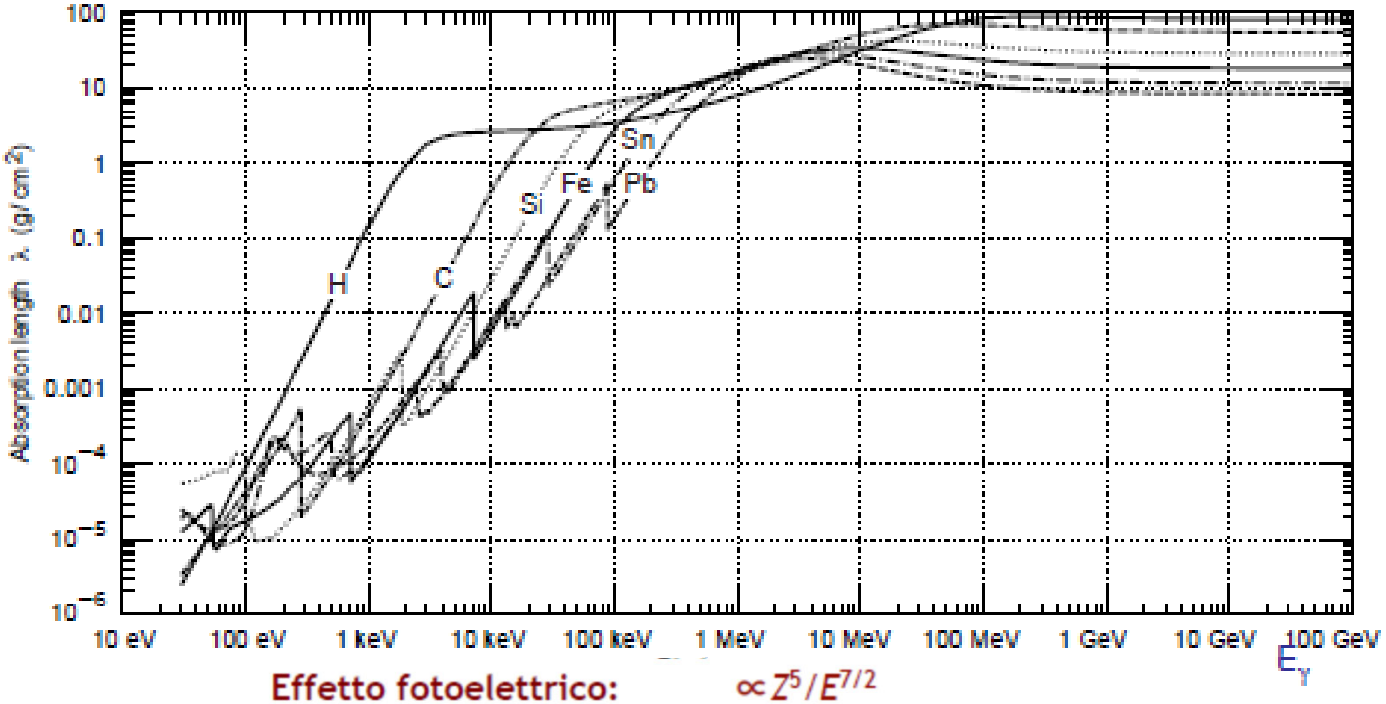

Effetto fotoelettrico: $\propto Z^5/E^{7/2}$

Effetto Compton $\propto Z/E$

Produzione di coppie: su nucleo $\propto Z^2$
su elettroni $\propto Z$

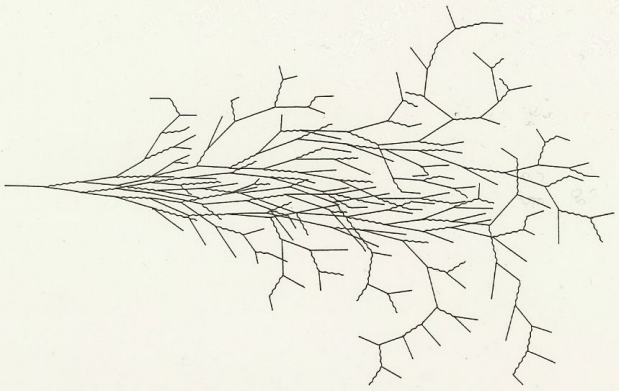

Fig. 7.20. Schematic representation of an electromagnetic cascade. The wavy lines are photons and the solid lines electrons or positrons.

Figure 11.2 Shower profiles in lead. The number of electrons should be multiplied by a normalization factor of 0.79. (D. Müller, Phys. Rev. D 5: 2677, 1972.)

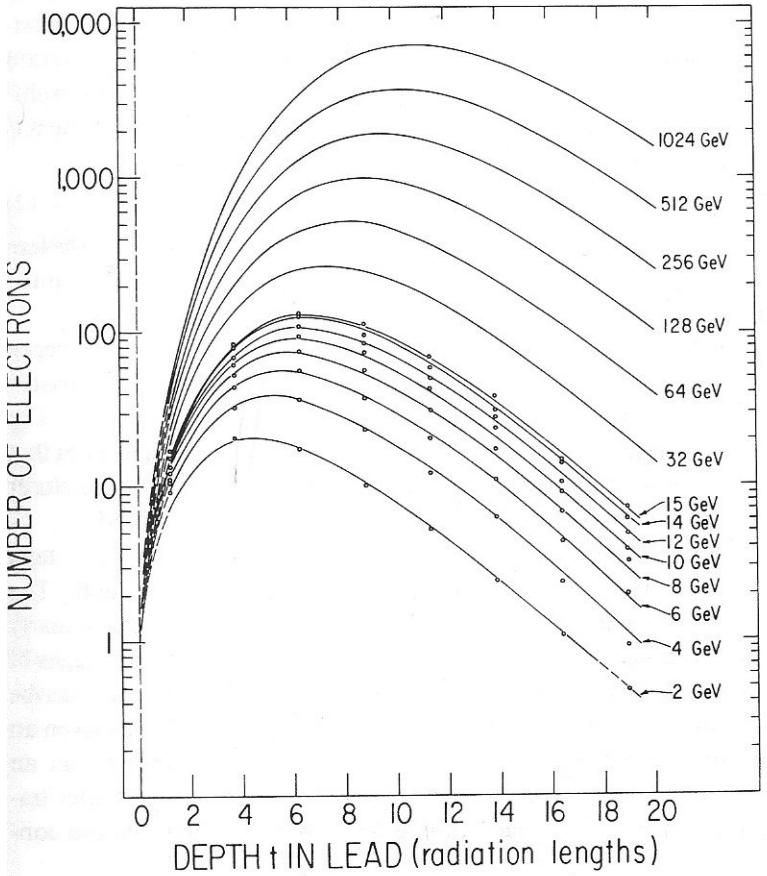

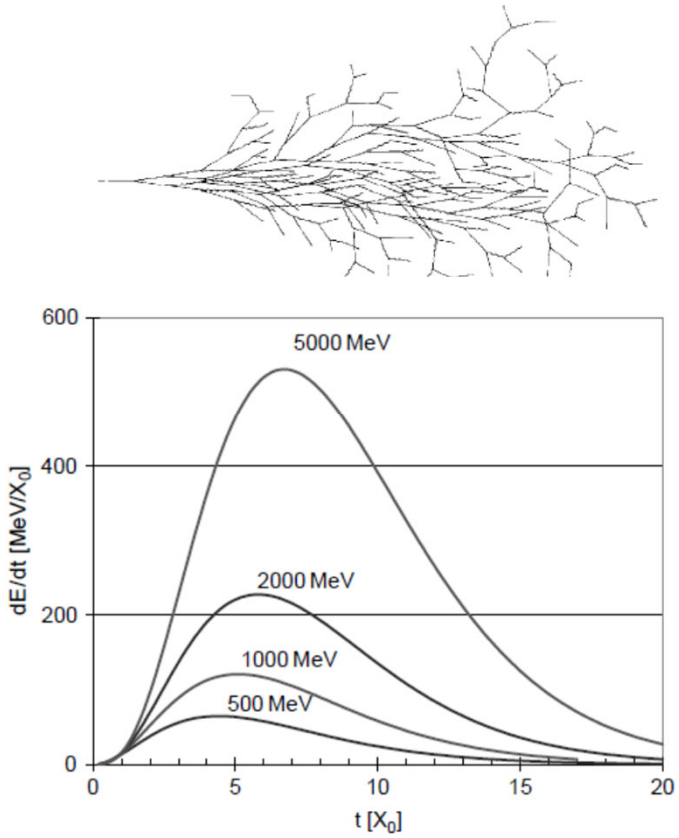

Svilupo longitudinale di una shower em.

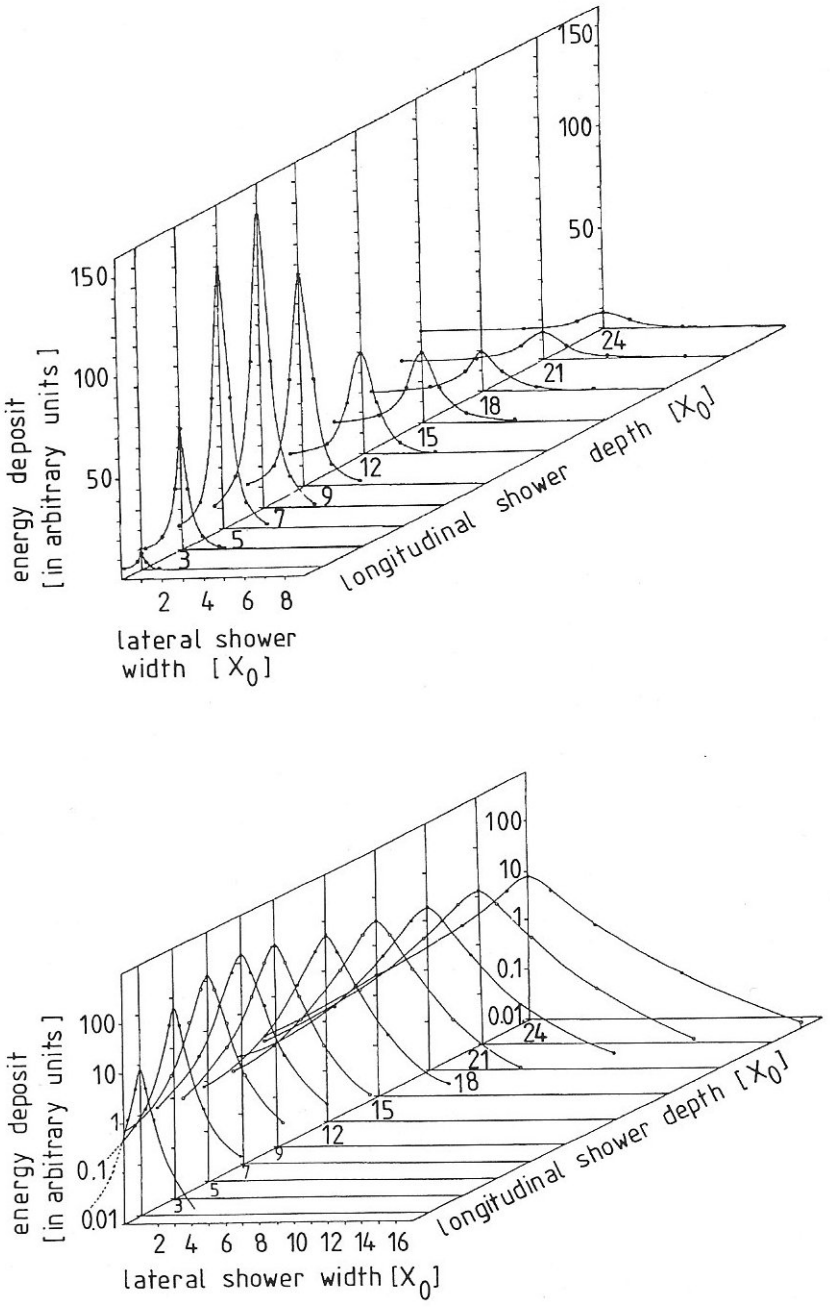

Fig. 7.23. Longitudinal and lateral development of an electron shower (6 GeV) in lead shown with linear and logarithmic scales (based on [504, 505]).

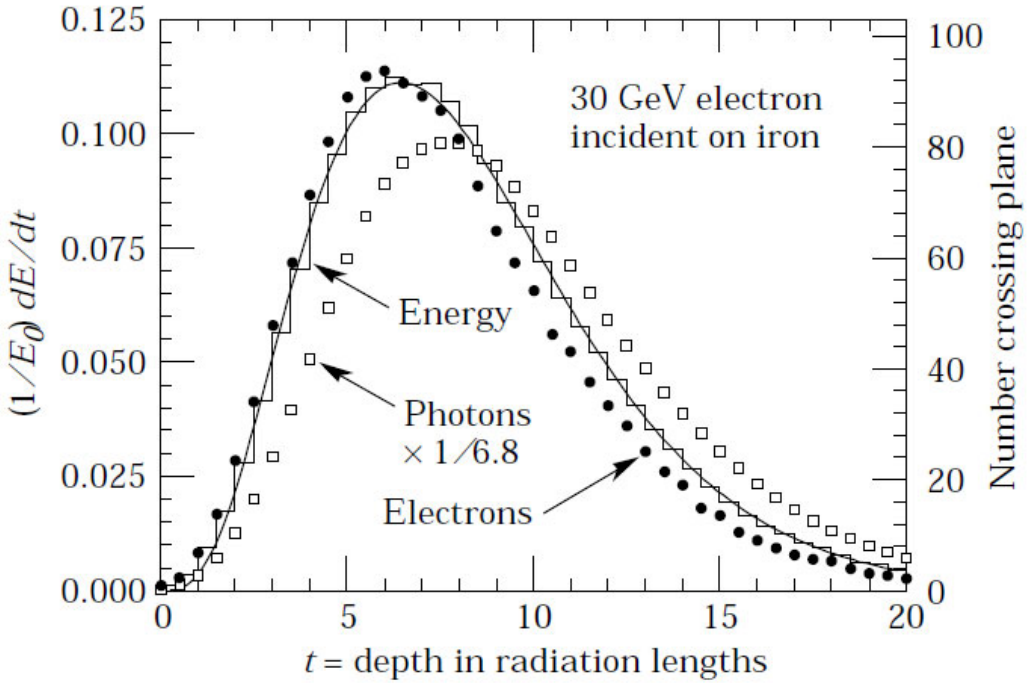

Figure 27.18: An EGS4 simulation of a 30 GeV electron-induced cascade in iron. The histogram shows fractional energy deposition per radiation length, and the curve is a gamma-function fit to the distribution. Circles indicate the number of electrons with total energy greater than 1.5 MeV crossing planes at $X_0/2$ intervals (scale on right) and the squares the number of photons with $E \geq 1.5$ MeV crossing the planes (scaled down to have same area as the electron distribution).

Un apparato che mi permette una misura di tracce (insieme di camere MWPC o a deriva o silici) posto in un campo magnetico (possibilmente uniforme) mi fornisce una misura dell'impulso delle particelle (misura di β dalla misura del raggio di curvatura).

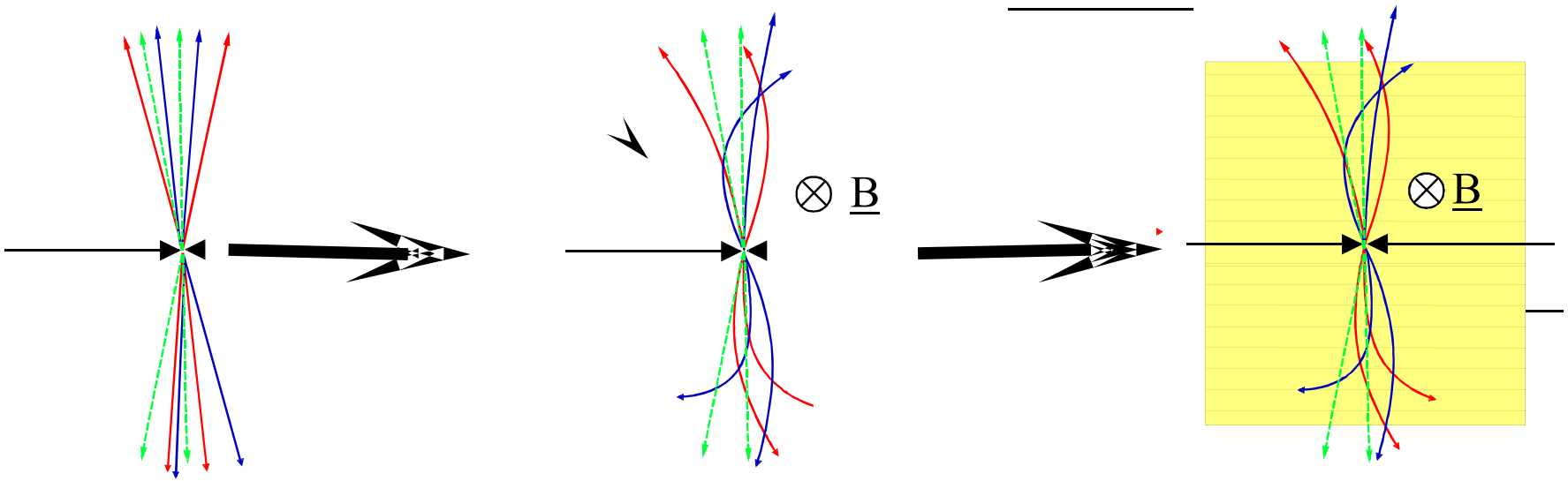

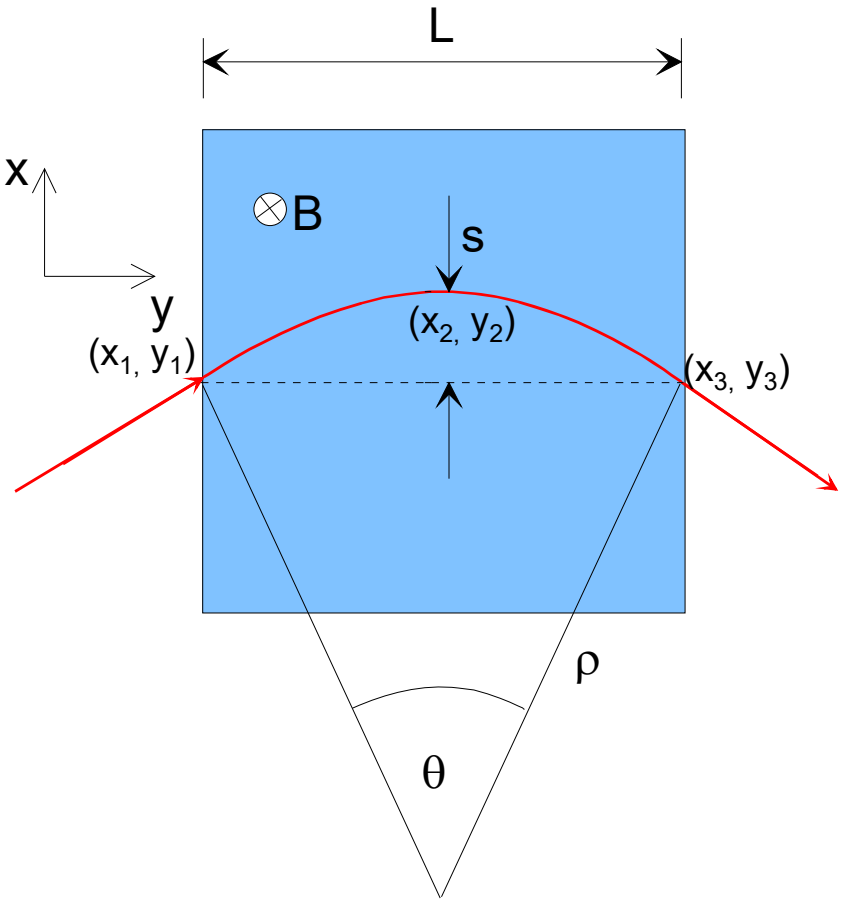
L
x
B
s
y
(x_2, y_2)
(x_1, y_1)
(x_3, y_3)
ρ
θ

Rappresentazione schematica di uno spettrometro magnetico

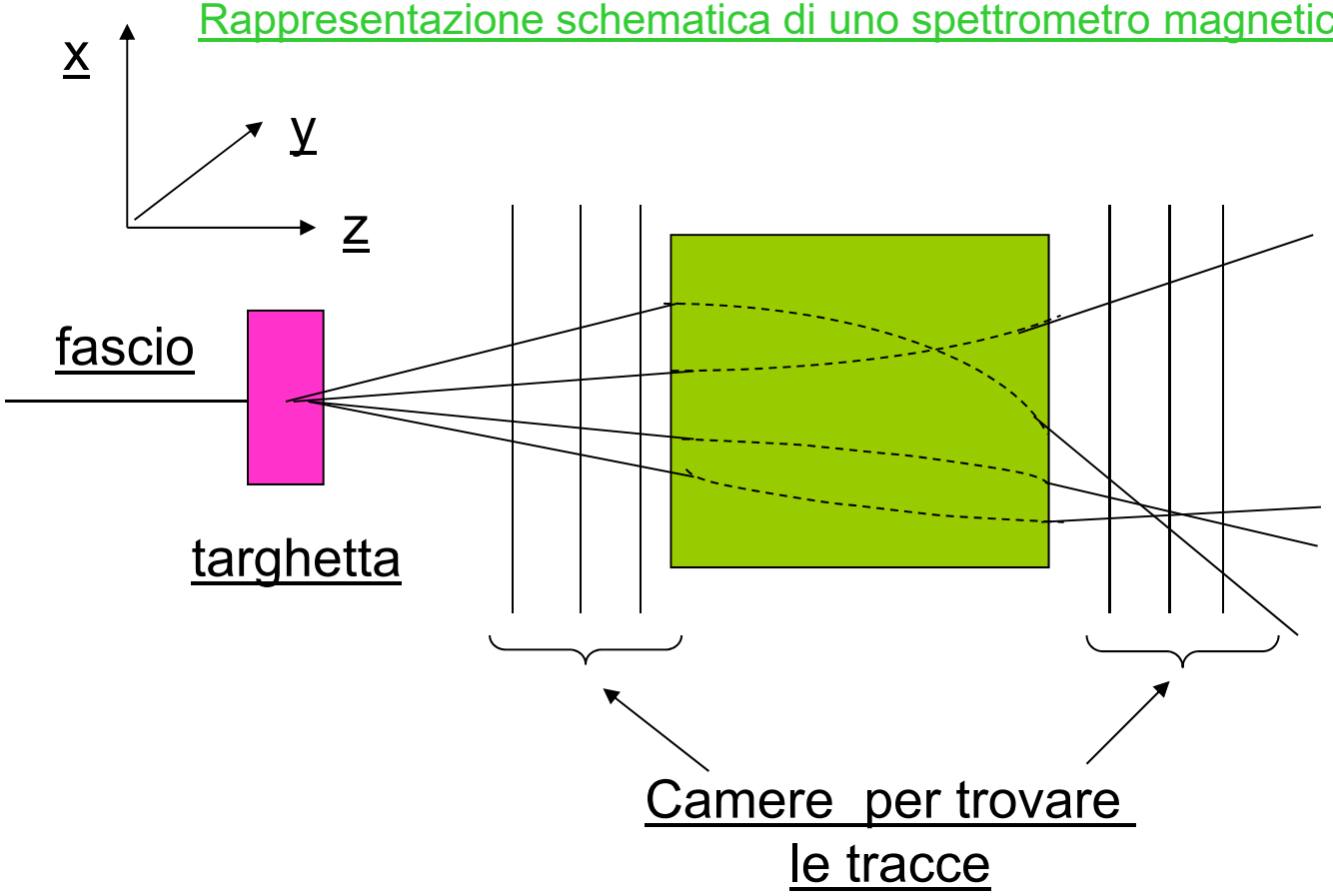

Misure di posizione

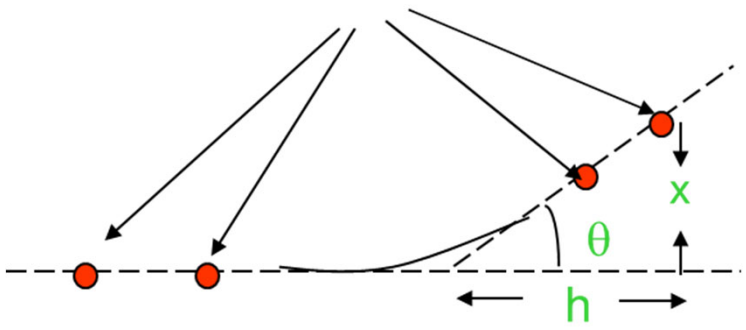

Figure 7.13 The time difference per unit flight path for πK, Kp, and πp as a function of momentum.

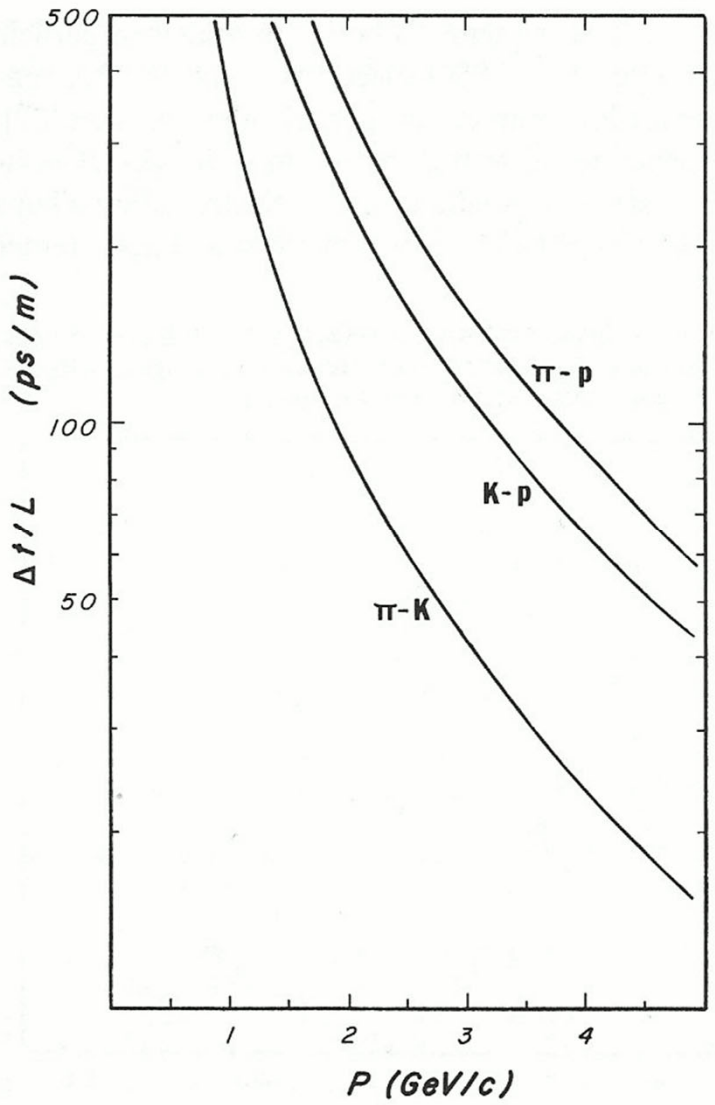

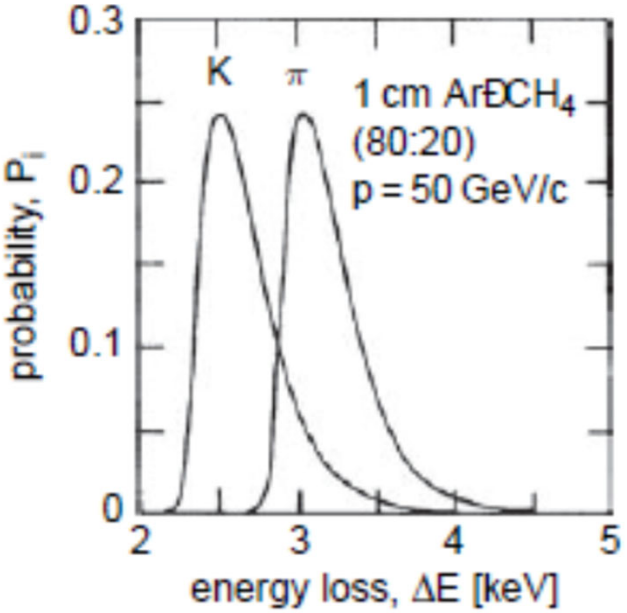

Distribuzione tipica di perdita di energia di pioni e kaoni energia di 50 GeV/c in uno strato di miscela di argon-metano di 1 cm

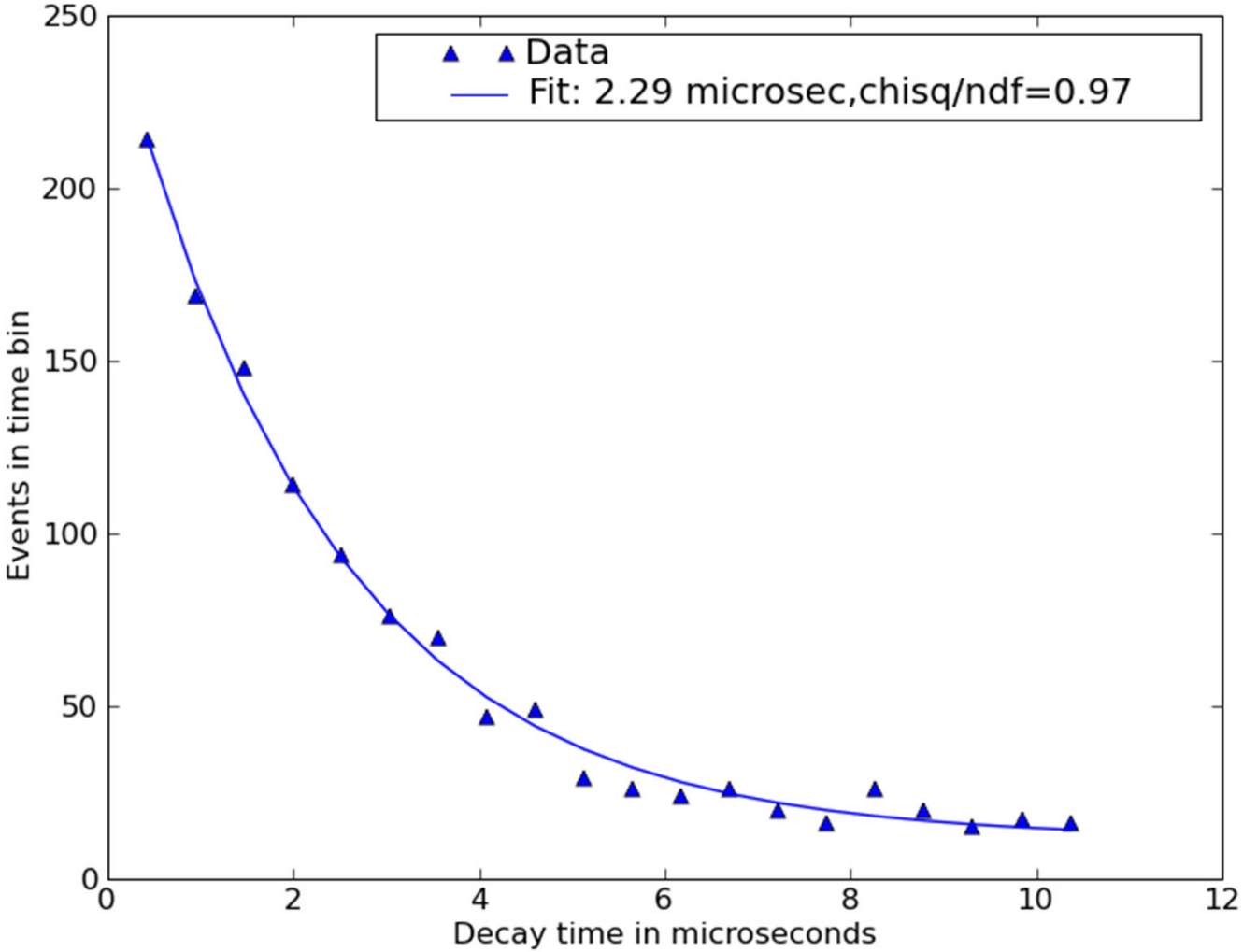
Data
Fit: 2.29 microsec,chisq/ndf=0.97
Events in time bin
Decay time in microseconds
0
50
100
150
200
250
0
2
4
6
8
10
12

Figure e note relative alle lezioni 7 ed 8 (Maggio 2019)

Rivelatori basati sulla ionizzazione

IONIZZAZIONE: indotta da particelle cariche: il passaggio delle particelle e' rivelato dalle ionizzazioni prodotte lungo il percorso della particella stessa.

Tecniche di visualizzazione di traccia

- Fondamentali nello sviluppo della fisica N. e SN. (inizialmente usando raggi cosmici poi presso acceleratori)

Ad es. nella scoperta di particelle con decadimento debole (v.m.τ~10^-10s) mediante osservazione decadimenti deboli con vertici di decadimento secondari a distanza misurabile (ctau…)

Tecniche visualizzanti (traccia + ionizzazione/dE/dx) + campo magnetico (impulso)

Tecniche elettroniche

- Raccolta ionizzazione e trasformazione in impulso elettrico.
- Alla base di tutti i moderni rivelatori ed apparati

Rivelatori di Tracce

Tecniche di visualizzazione di traccia

1) Camera a Nebbia (Wilson – 1912) :
un gas con **vapore sovrasaturo** produce goccioline dove sono presenti ioni a causa di una rapida espansione (asincrona nelle prime c.n., poi con trigger esterno). Si illumina e si fotografa la camera subito dopo l'espansione. Tipica risoluzione ≅ 0.5 mm.
Molte informazioni da densita' ionizzazione (dE/dx) e curvatura (impulso) se campo magnetico presente
Camera a diffusione: camera a nebbia senza variazione di pressione

Scoperta del Positrone

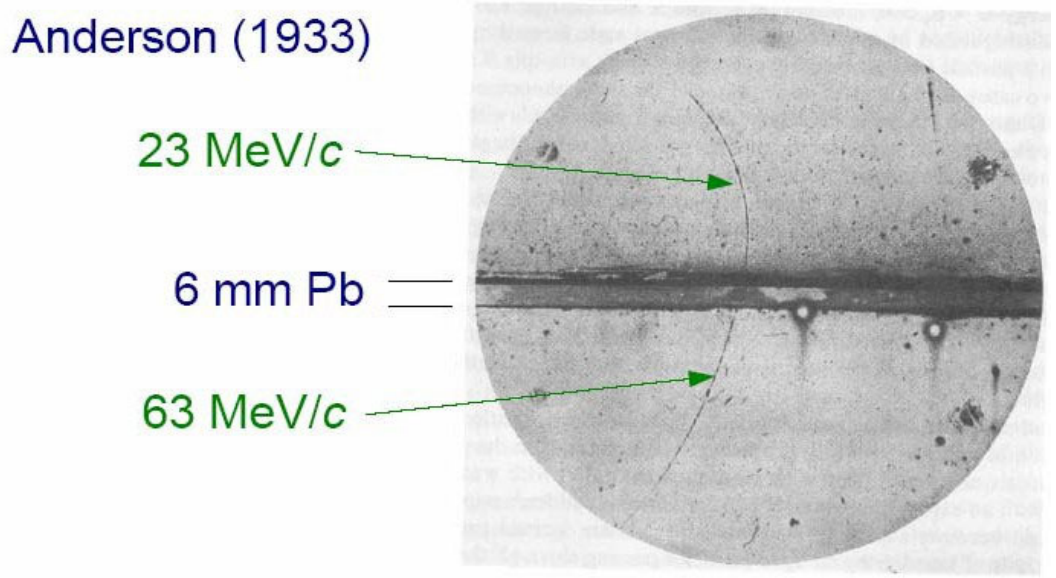

-Intensita' traccia→ densita' ionizzazione (dE/dx)
-Curvatura → impulso
→ massa

Evidenza particelle Lambda (V0)
Misura traccia + ionizzazione (dE/dx)
+ campo magnetico (impulso)

Rochester et al Nature, 1947 Evidence for a new unstable particle

Proiettile: Raggi cosmici energetici (penetranti)
Rivelatore: camera a nebbia

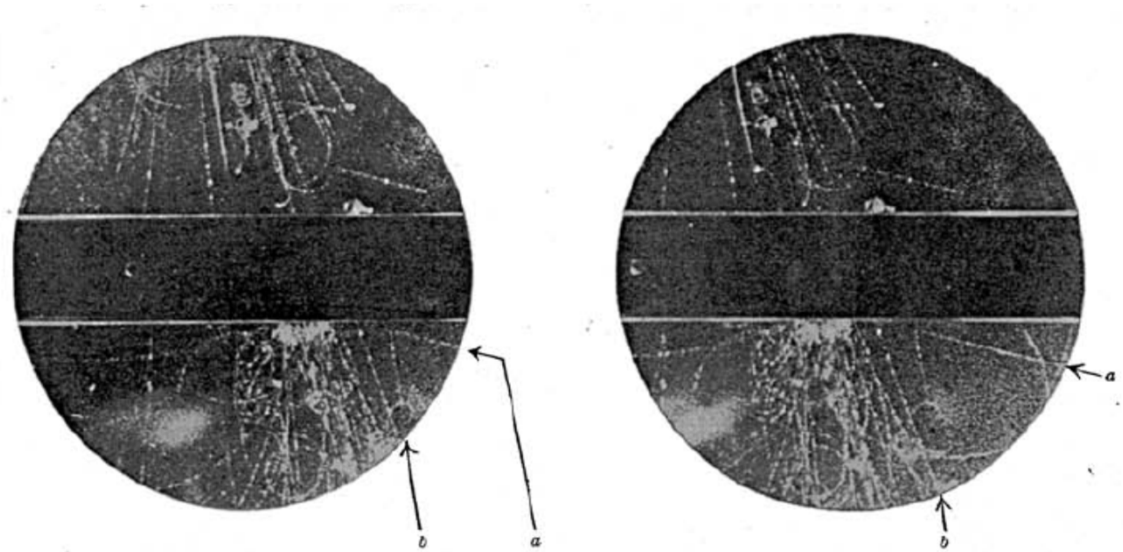

Fig. 1. Stereoscopic photographs showing an unusual fork (a b) in the gas. The direction of the magnetic field is such that a positive particle coming downwards is deviated in an anticlockwise direction

Primi fasci ad acceleratori: BNL Cosmotron (pi-):
new V0 evidence(Fowler et al)

Scoperta della stranezza

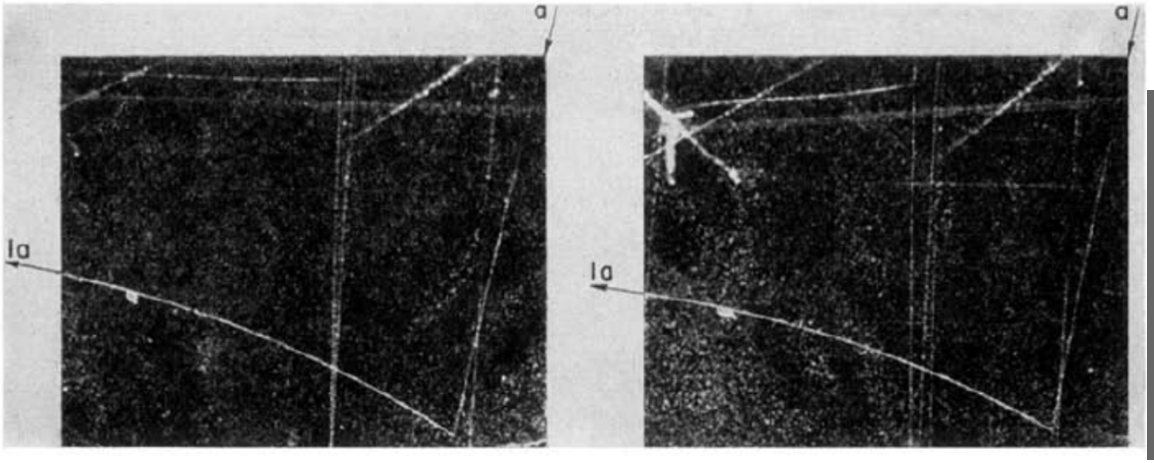

Fig. 4. Case F. Photograph of a negative unstable particle (a) best interpreted as a Λ^-. The decay product (1a) is identified as a π^- from momentum and ionization density.

These unstable particles were clearly produced with a large cross section, some percent of the cross section for producing ordinary particles, pions and nucleons.The puzzle was this: The new particles were produced in strong interactions and decayed into strongly interacting particles, but if the decays involved strong interactions, the particle lifetimes should have been ten orders of magnitude less than those observed…

Camera a nebbia: la nascita dell' antineutrino

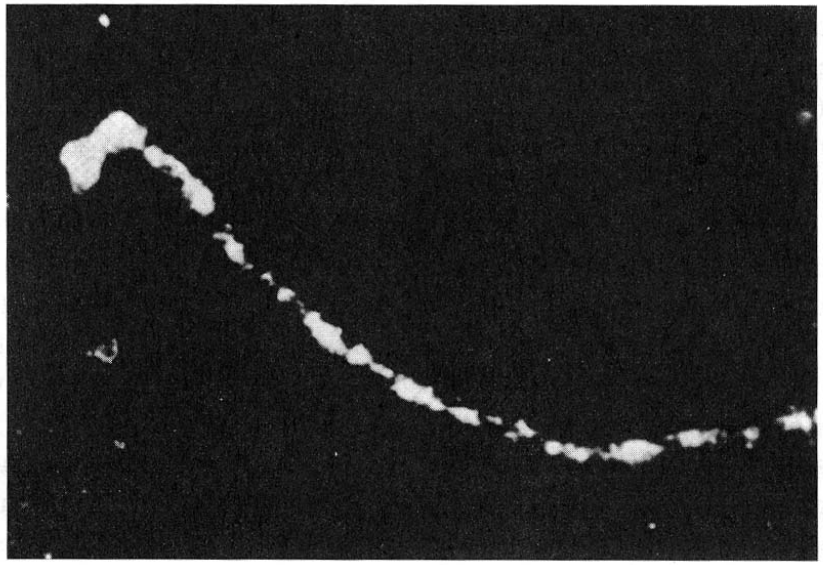

Fig. 1.1. Cloud chamber photograph of the birth of an antineutrino. It depicts the β-decay of the radioactive nucleus ^{6}He $\rightarrow$ ^{6}Li $+ e^- + \bar{\nu}_e + 3.5$ MeV. The long track is that of the electron, the short thick track that of the recoiling ^{6}Li nucleus. Some momentum is missing, and has to be ascribed to an uncharged particle (an antineutrino) travelling upwards in the picture (after Csikay and Szalay 1957). The cloud chamber consists essentially of a glass-fronted cylindrical tank of gas saturated with water vapour. Upon applying a sudden expansion by means of a piston at the rear of the chamber, the gas cools adiabatically and becomes supersaturated. Water vapour therefore condenses as droplets, preferentially upon charged ions created, for example, by the passage of a charged particle through the gas. The cloud chamber was invented by C.T.R. Wilson for a quite different purpose: to try to reproduce, in the laboratory, the 'glory' phenomenon he had observed on a Scottish mountain top. Wilson failed in this endeavour but by 1912 had given the world a valuable new technique for nuclear research.

Rivelatori di Tracce

Tecniche di visualizzazione di traccia

2)Camera a Bolle (Glaser– 1952):
un **liquido** (idrogeno, deuterio, elio….) in cui la **pressione** idrostatica è mantenuta per qualche millisecondo **più bassa della sua tensione di vapore**. Si formano delle **bollicine** lungo la traiettoria delle particelle a causa della presenza delle coppie e-ione che producono un aumento locale della temperatura.

Risoluzione spaziale da 300 a 20 μm.

SCOPERTA ANTI- NEUTRONE:

anti-p + p → anti-n + n
Annichilazione anti-n (stella con energia maggiore di 1.5 GeV)

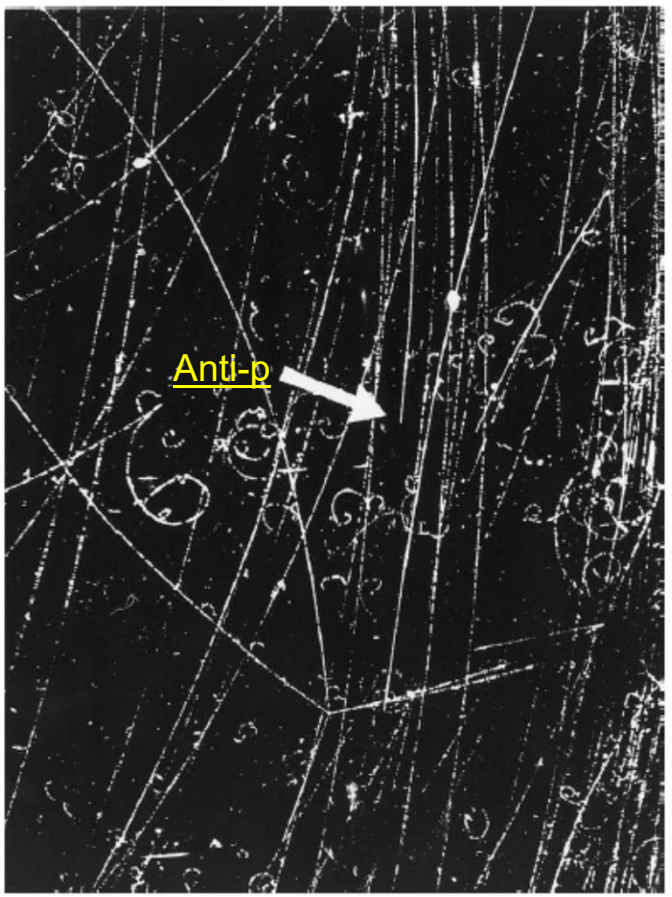

Figure 4.2. An antiproton enters the bubble chamber from the top. Its track disappears at the arrow as it charge exchanges, $p\bar{p} \rightarrow n\bar{n}$. The antineutron produces the star seen in the lower portion of the picture. The energy released in the star was greater than 1500 MeV. (Ref. 4.7)

Produzione di coppie in camera a bolle

γ (e) → e+ e- (e)

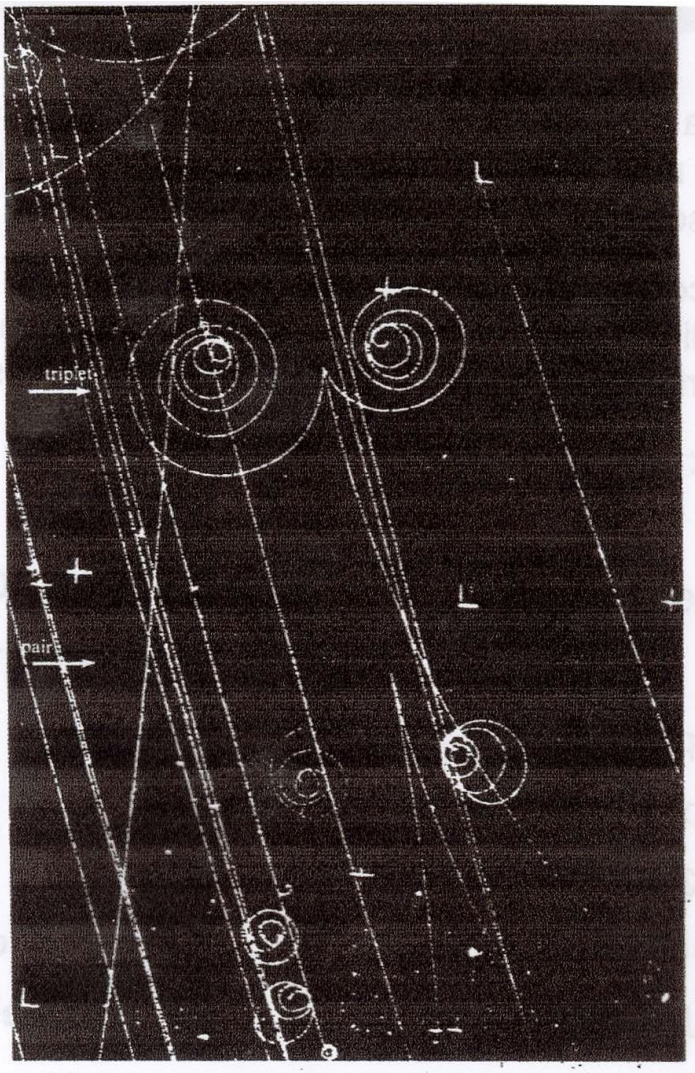

Figura 2.28. Formazione di una coppia elettrone-positrone nel campo di un elettrone (tripletto). Formazione di una coppia nel campo di un protone (coppia). (Camera a bolle a idrogeno). [Foto gentilmente concessa dal Lawrence Radiation Laboratory].

The discovery of the Ξ^0 did not take place until 1959. Since the Ξ has strangeness -2, its production by pions is quite infrequent: the minimal process would be $\pi^- p \rightarrow K^0 K^0 \Xi^0$. A more effective means is to start with a particle with strangeness -1. This was accomplished by L. Alvarez and co-workers using a hydrogen bubble chamber and a mass-separated beam of K^- mesons of momentum about 1 GeV/c produced by the Bevatron. Using the great analytical power of the bubble chamber technique, they were able to identify an event $K^- p \rightarrow K^0 \Xi^0$ (Ref. 3.20). The K^0 decayed into $\pi^+ \pi^-$. The Ξ^0 decayed into $\Lambda^0 \pi^0$. Both the decay of the K^0 and the decay of the Ξ^0 gave noticeable gaps in the bubble chamber pictures. The Λ^0 was identified by its charged decay mode, $\Lambda \rightarrow p\pi^-$. The last hyperon, Ω^-, was not discovered until 1964, as discussed in Chapter 5.

The bubble chamber was invented by Donald Glaser in 1953. The first chambers used propane and other liquid hydrocarbons. The idea was rapidly adapted by Luis Alvarez and his group who used liquid hydrogen (and later also deuterium) as the working liquid. They also developed methods for building increasingly large chambers. The bubble chamber works by producing a superheated liquid by rapid expansion just before (about 10 ms) the arrival of the particles to be studied. Bubbles are formed when boiling starts around the ions produced by the passage of the charge particles through the liquid. These bubbles are allowed to grow for about 2 ms at which time lights are flashed and the bubbles are photographed. The properties of bubble chambers are ideally suited for use with accelerators. At an accelerator, the arrival time of a particle beam is known. This allows one to expand the chamber before the arrival of the charged particles, which is not possible in cosmic-ray experiments.

Camera a Bolle: scoperta anti-Λ

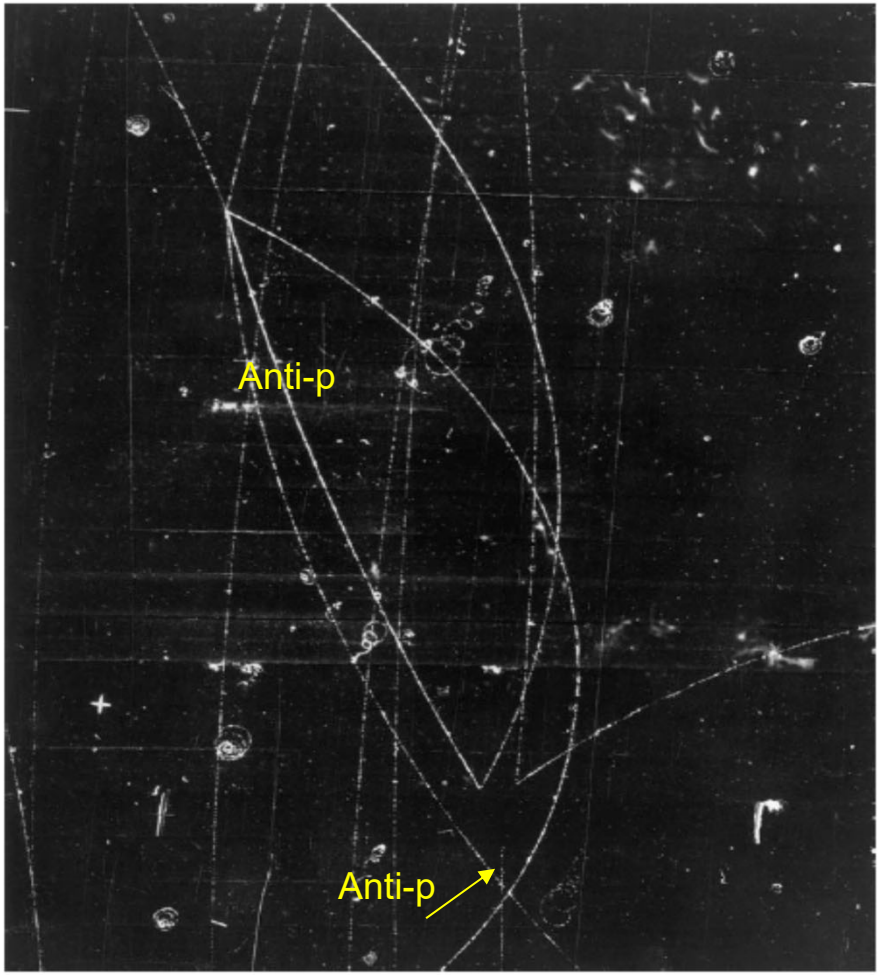

Figure 4.3. Production of a $\Lambda\overline{\Lambda}$ pair by an incident antiproton. The antiproton enters the chamber at the bottom and annihilates with a proton. The Λ and $\overline{\Lambda}$ decay nearby. The antiproton from the antilambda annihilates on the left-hand side of the picture and gives rise to a 4 prong star. The picture is from the 72-inch bubble chamber at the Bevatron. (Ref. 4.9)

Anti-p +p→ anti-Λ + Λ
(e successiva annichilazione anti-p)
Λ → $\pi-$ p
Anti-Λ → $\pi+$ anti-p

Scoperta di risonanze: Sigma(1385)

The full importance and wide-spread nature of resonances became clear only in 1960 when Luis Alvarez and a team that was to include A. Rosenfeld, F. Solmitz, and L. Stevenson began their work with separated K^- beams in hydrogen bubble chambers exposed at the Bevatron. The first resonance observed (**Ref.** 5.5) was the $I = 1$ $\Lambda\pi$ resonance originally called the Y_1^*, but now known as the $\Sigma(1385)$. The reaction studied in the Lawrence Radiation Laboratory's 15-inch hydrogen bubble chamber was $K^- p \rightarrow \Lambda\pi^+\pi^-$ at 1.15 GeV/c. The tracks in the bubble chamber pictures were measured on semiautomatic measuring machines and the momenta were determined from the curvature and the known magnetic field. The measurements were refined by requiring that the fitted values conserve momentum and energy. The invariant masses of the pairs of particles,

$$M_{12}^2 = (p_1 + p_2)^2 = (E_1 + E_2)^2 - (\mathbf{p_1} + \mathbf{p_2})^2 \qquad (5.8)$$

were calculated. For three-particle final states a Dalitz plot was used, with either the center-of-mass frame kinetic energies, or equivalently, two invariant masses squared, as variables. As for the τ-meson decay originally studied by Dalitz, in the absence of dynamical correlations, purely s-wave decays would lead to a uniform distribution over the Dalitz plot.

The most surprising result found by the Alvarez group was a band of high event density at fixed invariant mass, indicating the presence of a resonance.

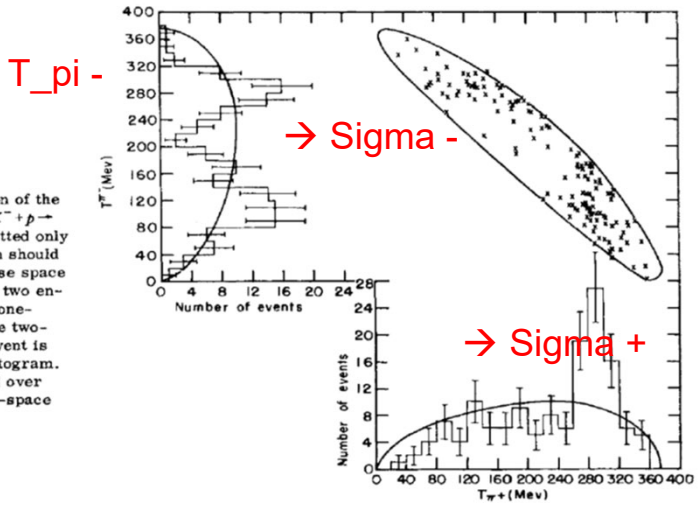

FIG. 1. Energy distribution of the two pions from the reaction $K^- + p \rightarrow \Lambda + \pi^+ + \pi^-$. Each event is plotted only once on the Dalitz plot, which should be uniformly populated if phase space dominated the reaction. The two energy histograms are merely one-dimensional projections of the two-dimensional plot, and each event is represented once on each histogram. The solid lines superimposed over the histograms are the phase-space curves.

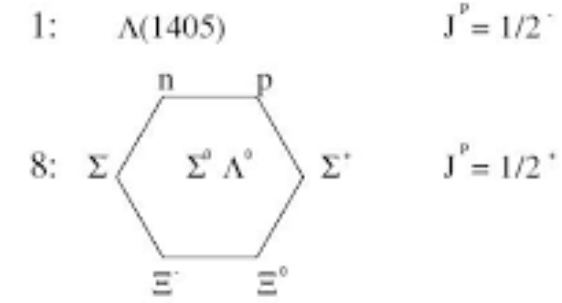

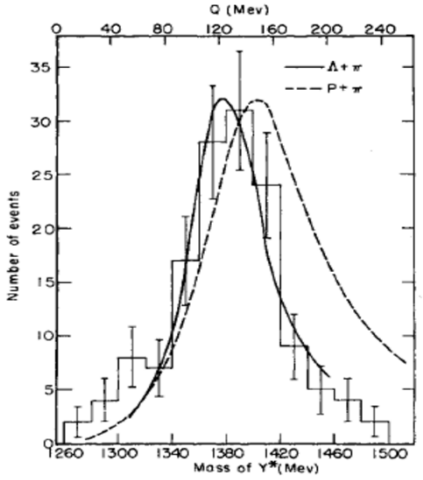

FIG. 2. Mass distribution for Y^* and fitted curves for $\pi\Lambda$ and πp resonances. The lower scale refers only to the $\pi\Lambda$ resonance. Q is the kinetic energy released when either isobar dissociates. The curve for the $\pi\Lambda$ resonances is fitted to the center eight histogram intervals of our data. The πp curve is the fit obtained by Gell-Mann and Watson,[7] to πp scattering data. Both fits are to the formula $\sigma \propto \lambda^2 \Gamma^2/[(E - E_0)^2 + \frac{1}{4}\Gamma^2]$, where $\Gamma = 2b(a/\lambda)^3/[1 + (a/\lambda)^2]$.

Rivelatori di Tracce

A) Tecniche Visualizzanti

3) Emulsioni Nucleari (Powell– 1939):
costituite da grani di AgBr (bromuro di argento) immersi in gelatine con
densità di alcuni grani / μm . La particella produce elettroni che trasformano i grani in Argento metallico.

Risoluzione spaziale ≅ 1 μm .

Emulsioni: scoperta del pione carico

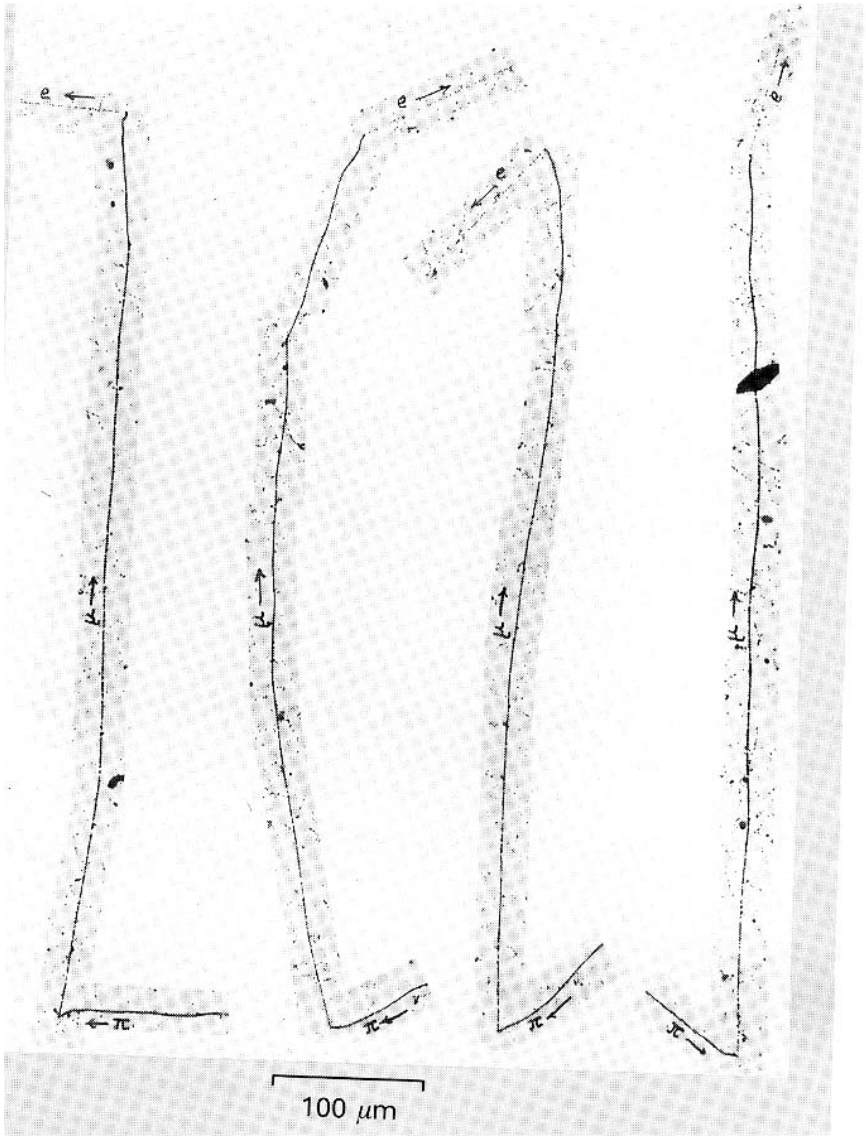

Fine lezione 8 maggio

Anti-proton star

Chamberlain et al, Phys. Rev 101 (1956)

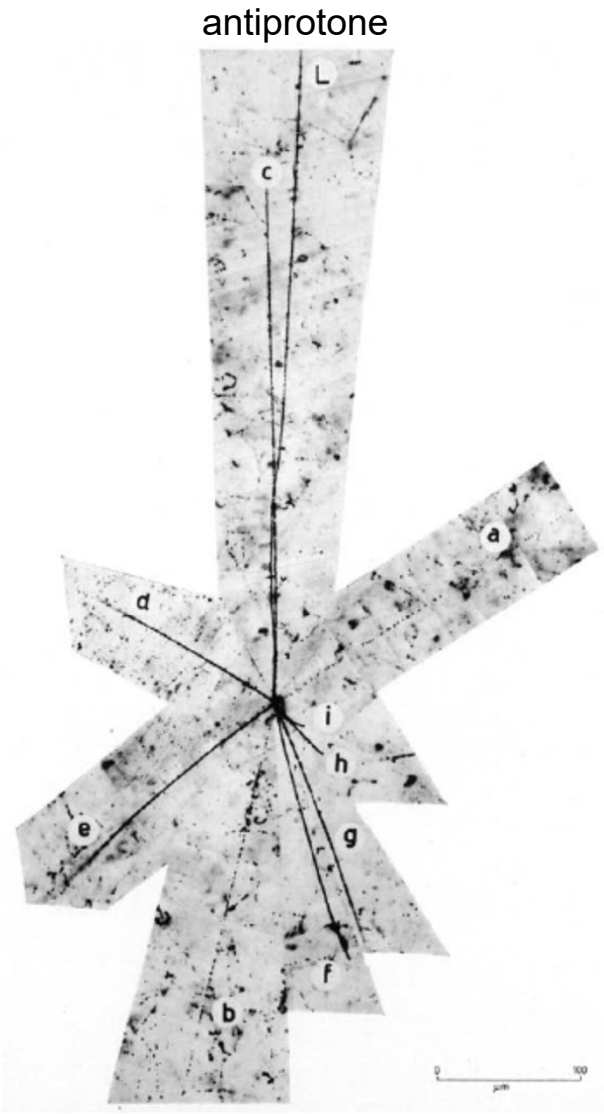

Figure 4.1. The first antiproton star observed in an emulsion. The incident antiproton is track L. The light tracks *a* and *b* are pions. Track *c* is a proton. The remaining tracks are protons or alpha particles. The exposure was made at the Bevatron. (Ref. 4.2)

Scoperta della stranezza:

Iperone Sigma+ → p pi0 =>

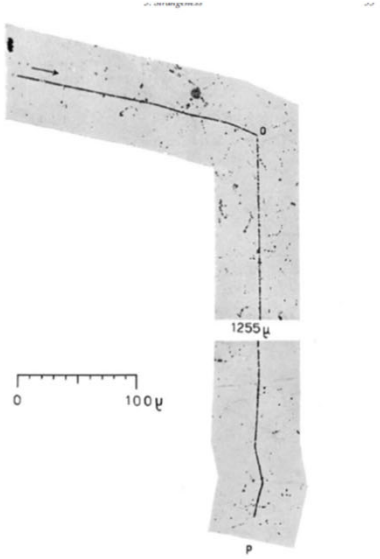

Figure 3.4. An emulsion event with a Σ^+ entering from the left. The decay is $\Sigma^+ \rightarrow p\pi^0$. The p is observed to stop after 1255 μm. (Ref. 3.8)

Scoperta Primo ipernucleo

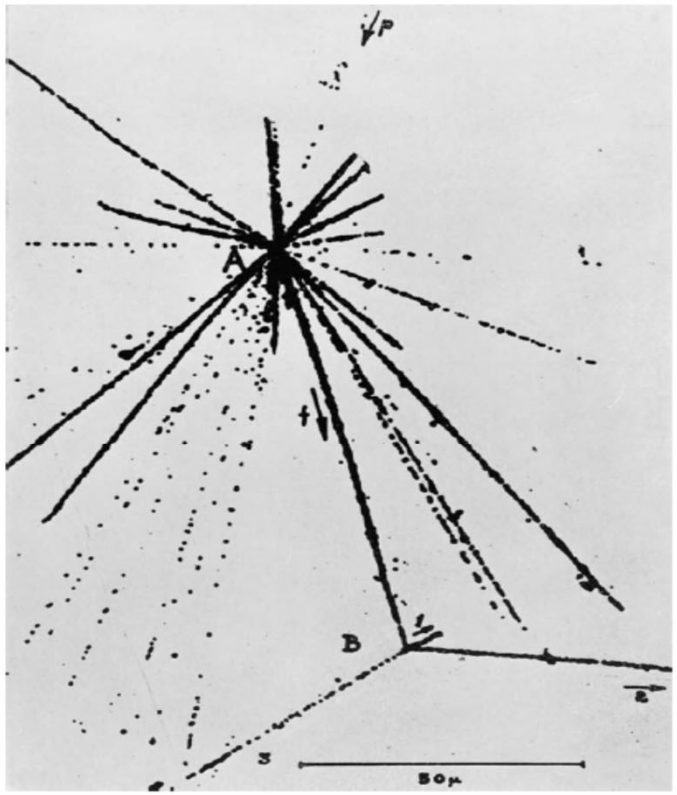

Figure 3.5. The star at A is caused by a cosmic-ray (marked p) incident from above colliding with a silver or bromine atom in the emulsion. The track f is due to a nuclear fragment with charge about 5. Its decay at point B shows that it contained a hyperon. The scale at the bottom indicates 50 μm. (Ref. 3.10)

(traccia f, creata dall'arrivo di un raggio cosmico su di un nucleo)

Rivelatori di Tracce

4) Camera a Scintille (1950) […primi passi verso rivelatori elettronici]
lastre conduttrici separate di 1 cm connesse a tensione ed a massa in modo alternato ad un generatore IMPULSIVO di tensione.
Tra le lastre vi è un gas NOBILE (He, Ne) che viene ionizzato dal passaggio della particella carica. Dopo il passaggio viene impulsato un campo elettrico di ~10KV/cm che accelerando gli elettroni innesca una scarica lungo tutta la traccia di ionizzazione lasciata dalla particella. Le scintille sono nel visibile e vengono fotografate.
Risoluzione spaziale ≤ 1 mm.

Figure 12.2 Principles of spark chamber operation. (S) Scintillation counter, (Co) coincidence circuit, (A) amplifier, and (sg) spark gap.

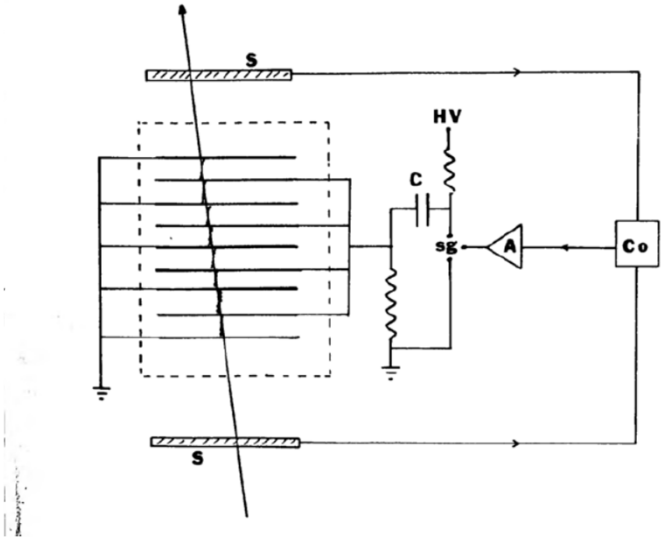

Melvin Schwartz one of the co-discoverers of the muon neutrino with a spark chamber used in its discovery.

Rivelatori di Tracce tramite ionizzazione

B) Tecniche Elettroniche

I rivelatori visualizzanti (c. nebbia, c.bolle,…) richiedono di **fotografare tutti gli eventi** e analizzarli in seguito. Sono pertanto sistemi **inefficenti e lenti.**

Nei rivelatori che utilizzano invece tecniche elettroniche , la carica elettrica, prodotto della ionizzazione dovuta al passaggio della particella, **viene raccolta con opportuni campi elettrici e trasformata in un segnale elettrico** che viene poi elaborato e salvato.

La modalita' di raccolta puo' essere **diretta** (camera a ionizzazione), **amplificata** mediante moltiplicazione della carica (camera proporzionale) o **saturata** (contatore Geiger)

Il materiale può essere GAS, LIQUIDO o SOLIDO.

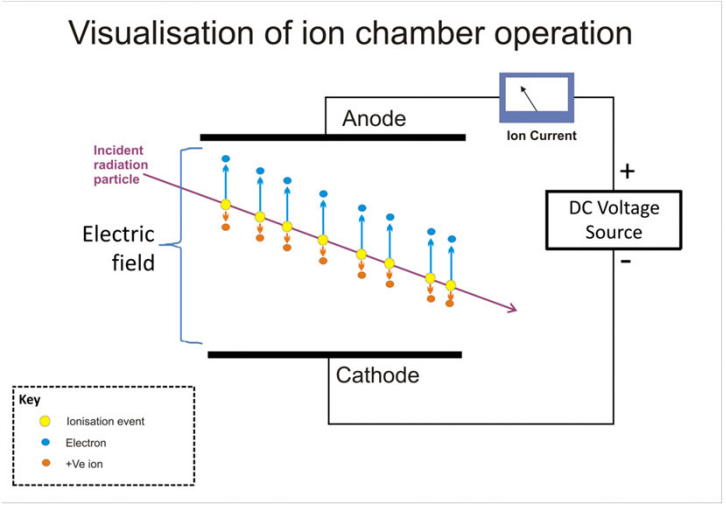

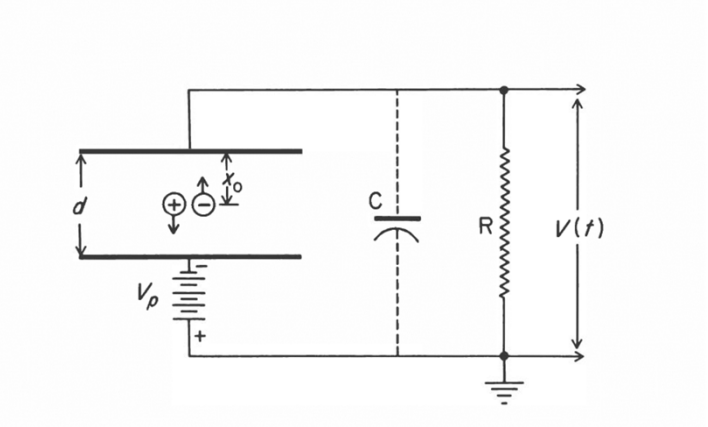

Rivelatori di Tracce tramite ionizzazione

Varie tipologie (metodi, tecniche, geometrie,…):

1) **camere a fili**: veloci, buona risoluzione spaziale (≅ 0.3 – 0.5 mm), self-triggering; informazione energia; usate in UA1 (Rubbia), fondamentali nella scoperta W,Z0.

2) **camere a deriva in gas**: coordinata pto passaggio basata su misura tempo raccolta della carica. Risoluzione spaziale ≅ 50 – 200 μm

3) TPC (Camera a proiezione temporale): Camere deriva + proporzionali

4) **Camere a deriva in semiconduttori**: resa 3 eV per coppia; risoluzione spaziale ≅ 10 μm.

Camere a fili: Multi wire proportional chambers

Varie tipologie:

1) **camere a fili**: veloci, buona risoluzione spaziale (≅ 0.3 – 0.5 mm), self-triggering; informazione energia; usate in UA1 (Rubbia), fondamentali nella scoperta W,Z0.

(G. Charpak et al., Nobel prize 1992)

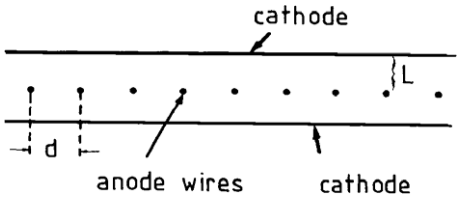

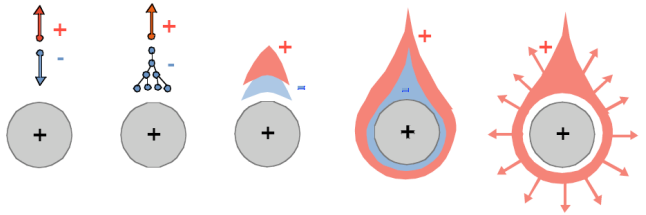

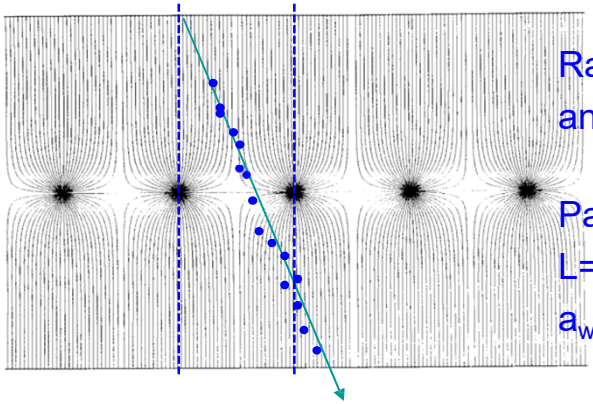

Raccolta elettroni sui fili anodici vicini.

Parametri tipici:
L=5mm, d=1mm,
a_{wire}=20mm.

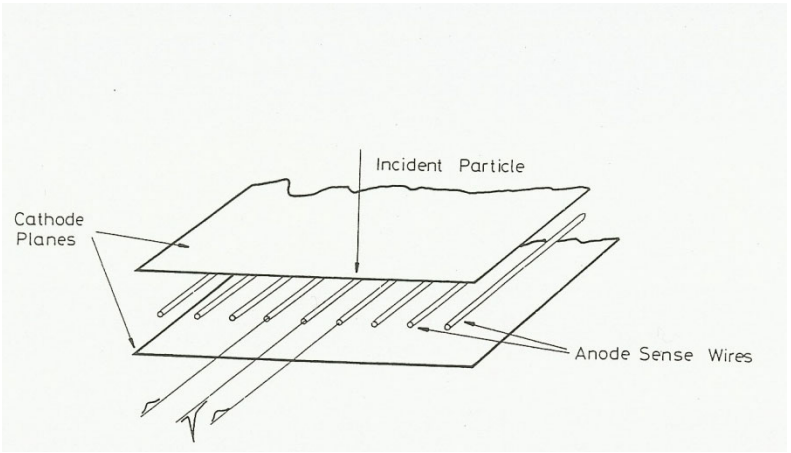

Lettura digitale: la risoluzione spaziale e' limitata a:

$$\sigma_x \approx \frac{d}{\sqrt{12}}$$

(d=1mm, σ_x=~300 μm)

Multi wire proportional chambers

Molti tracciatori (spettrometri,…)
basati su camere a fili

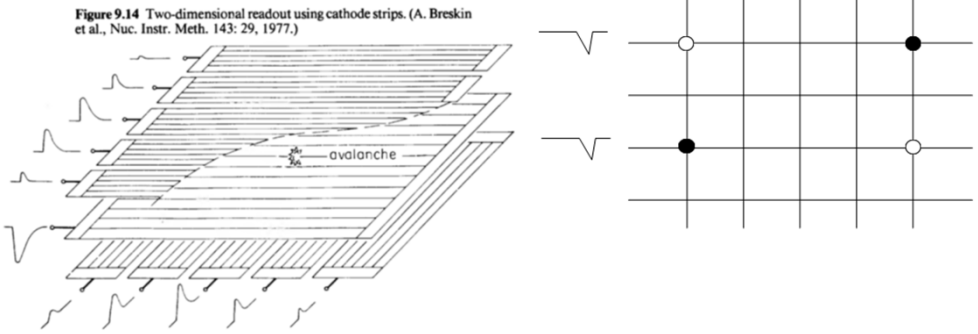

Figure 9.14 Two-dimensional readout using cathode strips. (A. Breskin et al., Nuc. Instr. Meth. 143: 29, 1977.)

2) camere a deriva in gas: coordinata pto passaggio basata su misura tempo raccolta della carica. Risoluzione spaziale ≅ 50 – 200 μm

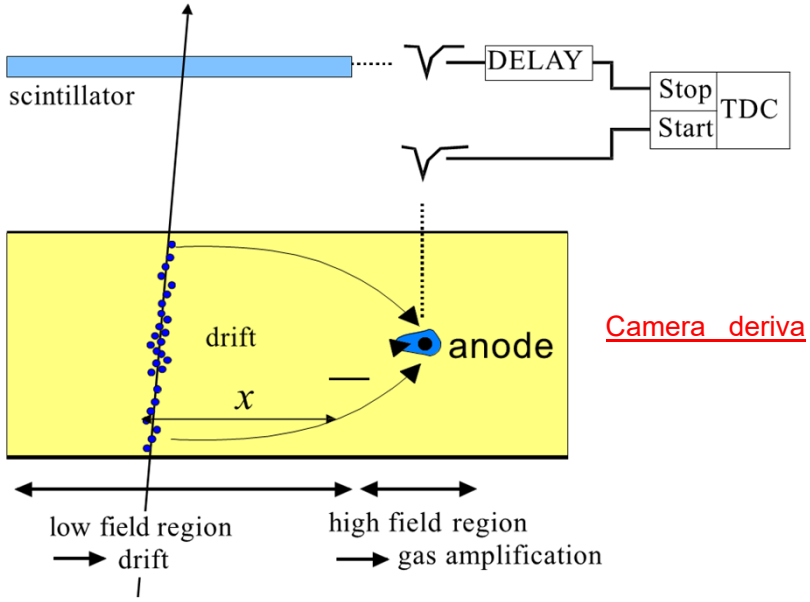

Camera deriva

♦ Misura il tempo di arrivo degli elettroni al filo a tensione relativo a t_0

$$x = \int v_D(t)dt$$

Camere a ionizzazione a semiconduttori:

3 eV per coppia; risoluzione spaziale < ≅ 10 μm.

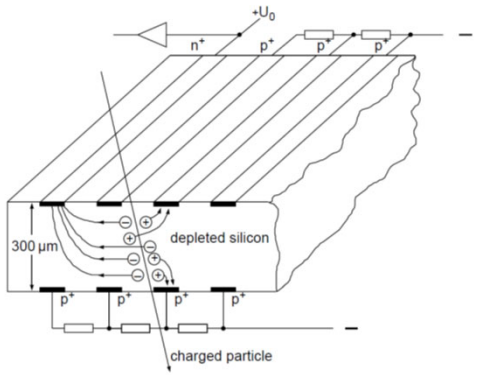

Fig. 7.42. Silicon drift chamber with graded potential [100, 117–119].

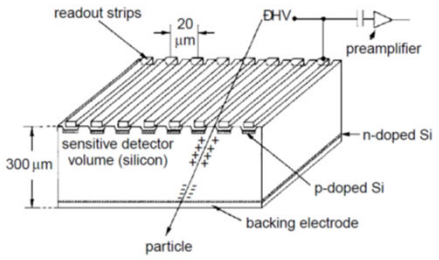

Fig. 7.39. Schematic layout of the construction of a silicon microstrip detector. Each readout strip is at negative potential. The strips are capacitively coupled (not to scale, from [103]).

TPC: Camere a proiezione temporale

TPC (Camera a proiezione temporale): Camere deriva + proporzionali
~("camera a nebbia elettronica")

Time Projection Chambers (TPC)

Large volume active detector.
full 3-D track reconstruction
x-y from wires and segmented cathode of MWPC
z from drift time
and
dE/dx

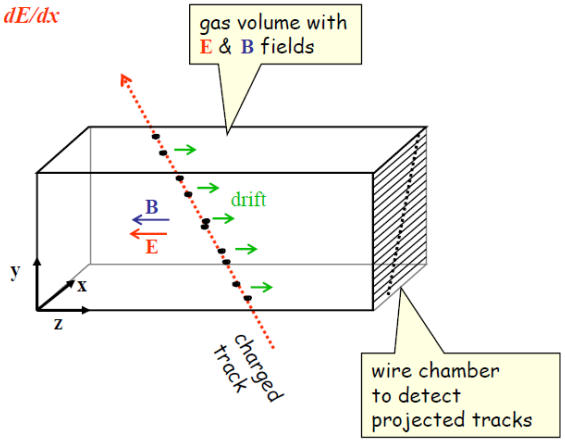

TPC: Camere a proiezione temporale

TPC (Camera a proiezione temporale): Camere deriva + proporzionali
~("camera a bolle elettronica")

Time Projection Chambers (TPC)

Large volume active detector.
full 3-D track reconstruction
x-y from wires and segmented cathode of MWPC
z from drift time
and
dE/dx

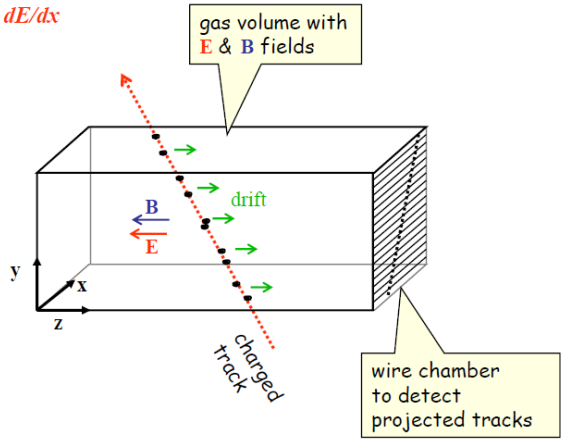

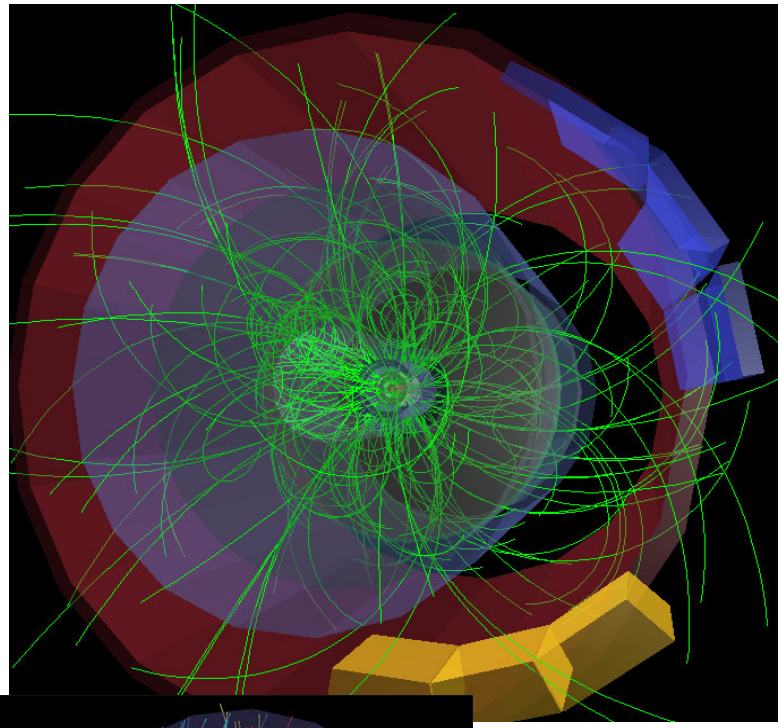

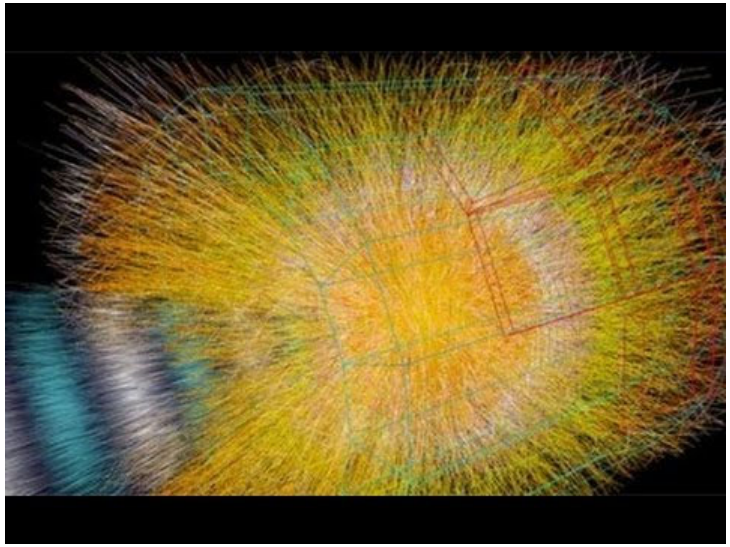

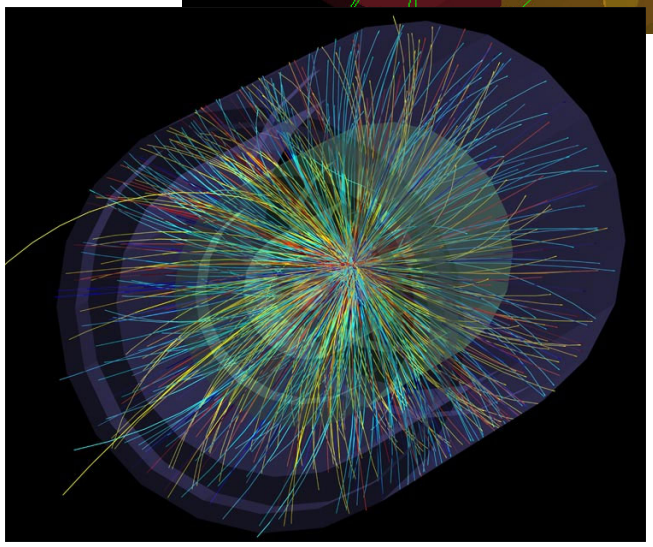

Eventi ricostruiti
dalla tpc di ALICE

Rivelatori basati sull'eccitazione

ECCITAZIONE: Indotta da particelle cariche su materiali scintillanti (stati metastabili con tempi di risposta da 10^{-9} a 10^{-6} secondi) che emettono fotoni di qualche eV (FLUORESCENZA).

i) Scintillatori inorganici : $X_0 \cong 2.6$ cm ; $\rho = 3.7$ gr cm^{-3}; risposta $\cong 10^{-7}$ s; resa energetica ; 1γ / 25 eV.

ii) Scintillatori organici : $X_0 \cong$ 30-40 cm; $\rho = 1$ gr cm-3; risposta $\cong 10^{-9}$ s; resa energetica : 1 γ / 100-500 eV.

Molto utilizzati per definire un trigger e per misure di tempi (organici) e di energia (inorganici) e rivelatori di gamma (inorganici) [e per rivelazione $\pi 0$,…]

… e molti altri tipi di rivelatori (Cherenkov, di radiazione di transizione, calorimetri,…) che trasformano l'energia rilasciata in un segnale elettrico da leggere, misurare,…